University of Tennessee, Knoxville

TRACE: Tennessee Research and Creative Exchange

Masters Theses

Graduate School

12-1998

Variation of the aerosol optical depth at the ARM CART site

Terra Michelle Nash

Follow this and additional works at: https://trace.tennessee.edu/utk_gradthes

Recommended Citation

Nash, Terra Michelle, "Variation of the aerosol optical depth at the ARM CART site. " Master's Thesis, University of Tennessee, 1998.
https://trace.tennessee.edu/utk_gradthes/10327

This Thesis is brought to you for free and open access by the Graduate School at TRACE: Tennessee Research and Creative Exchange. It has been accepted for inclusion in Masters Theses by an authorized administrator of TRACE: Tennessee Research and Creative Exchange. For more information, please contact trace@utk.edu.

To the Graduate Council:

I am submitting herewith a thesis written by Terra Michelle Nash entitled "Variation of the aerosol optical depth at the ARM CART site." I have examined the final electronic copy of this thesis for form and content and recommend that it be accepted in partial fulfillment of the requirements for the degree of Master of Science, with a major in Environmental Engineering.

Wayne T. Davis, Major Professor

We have read this thesis and recommend its acceptance:

Terry Miller, Meng-Dawn Cheng

Accepted for the Council:
Carolyn R. Hodges

Vice Provost and Dean of the Graduate School

(Original signatures are on file with official student records.)

To the Graduate Council:

I am submitting herewith a thesis written by Terra Michelle Nash entitled "Variations in the Aerosol Optical Depth at the ARM CART Site." I have examined the final copy of this thesis for form and content and recommend that it be accepted in partial fulfillment of the requirements for the degree of Masters of Science, with a major in Environmental Engineering.

Wayne T. Davis, Major Professor

We have read this thesis
And recommend its acceptance:

Cheng, Meng-Dao

Terry L. Miller

Accepted for the Council:

Associate Vice Chancellor and
Dean of The Graduate School

Variation of the Aerosol Optical Depth at the ARM CART Site

A Thesis

Presented for the

Master of Science

Degree

The University of Tennessee, Knoxville

Terra Michelle Nash

December 1998

ACKNOWLEDGMENTS

The author wishes to thank Dr. Wayne T. Davis, Dr. Terry Miller and Dr. Meng-Dawn Cheng for their comments, support, encouragement and knowledge. Also thanks to Tasnima Apol and Christine Arenal for their editorial support. In addition, thanks to E. Scott Kopetz for his programming efforts on this project.

Thanks to the ORISE Professional Internship Program that provided the author with the opportunity to do research at Oak Ridge National Laboratory. This research was partially funded by the US Department of Energy ARM program. All work was done at Oak Ridge National Laboratory, managed by Lockheed Martin Energy Research Corp. For the U.S. Department of Energy under contract number DE-AC05-96OR22464

Data were obtained from the Atmospheric Radiation Measurement Program sponsored by the U.S. Department of Energy Research, Office of Health and Environmental Research, Environmental Sciences Division. The author thanks the ARM Archive staff, especially Debbie Shepherd, for their excellent assistance retrieving the massive MFRSR data files.

ABSTRACT

Atmospheric aerosols are an important factor in the global radiation budget and greenhouse warming effect. Aerosols contribute to atmospheric pollution and degradation of visibility. In an effort to better characterize the variations in the columnar aerosol loading, the aerosol optical depth (AOD) has been computed for five of the Atmospheric Radiation Measurement (ARM) Southern Great Plains (SGP) Cloud and Radiation Testbed (CART) facilities. Characterization of the AOD shows clear evidence that the spatial and temporal variations exist at a much finer scale than those of the CART site. The AOD measurements are indicators of atmospheric pollution and reduced visibility, and are used as inputs to radiative transfer models and research-grade Global Climate Models (GCM). The significant variations of the sub-GCM grid AOD cannot be ignored if the GCM are to be used to accurately predict future climate change.

TABLE OF CONTENTS

1. INTRODUCTION **1**

2. DESCRIPTION OF SITE AND DATA **4**

3. THEORY AND METHODOLOGY **10**

TOTAL OPTICAL DEPTH (TOD) 11
RAYLEIGH OPTICAL DEPTH (ROD) 14
OZONE OPTICAL DEPTH (O3OD) 15

4. RESULTS AND DISCUSSION **17**

CASE STUDIES 17
January 28, 1997 ..... *18*
April 3, 1997 ..... *22*
June 17, 1996 ..... *22*
October 23, 1996 ..... *26*
AOD 31
Basic Characteristics of AOD *31*
Time Dependent Structure *33*
Annual 33
Seasonal/Monthly 34
Daily Variation 41
Morning /Afternoon 44
Spatial Variation *45*

5. CONCLUSIONS AND RECOMMENDATIONS **52**

REFERENCES **53**

APPENDIX **56**

VITA **58**

LIST OF TABLES

Table 1. AOD by Facility at 500 nm 33
Table 2. Morning versus Afternoon AOD 44
Table 3. Pair-wise Pearson Coefficients for All AOD 47
Table 4. PCA Eigenvalues for all AOD 48
Table 5. PCA Factor Loadings for all AOD 48
Table 6. Pearson Correlation Coefficients: Morning and Afternoon 49
Table 7. PCA Eigenvalues for Morning AOD 49
Table 8. PCA Factor Loadings for Morning AOD 50
Table 9. PCA Eigenvalues for Afternoon AOD 50
Table 10. PCA Factor Loadings for Afternoon AOD 51

LIST OF FIGURES

Figure 1. Map of ARM AGP CART Site with Facilities of Interest as Solid Circles ..5
Figure 2. The Multi-Filter Rotating Shadowband Radiometer 6
Figure 3. Example of Direct Normal Narrowband Irradiance with Clear Skies 8
Figure 4. Example of Direct Normal Narrowband Irradiance with Cloudy Skies 9
Figure 5. Light Travel Through the Atmosphere 12
Figure 6. Direct Irradiance on January 28, 1997 19
Figure 7. Langley Plot on the Morning of January 28, 1997 20
Figure 8. Langley Plot with LMS on Morning of January 28, 1997 21
Figure 9. Direct Irradiance on April 3, 1997 23
Figure 10. Langley Plot on Morning of April 3, 1997 24
Figure 11. Direct Irradiance on June 17, 1996 25
Figure 12. Langley Plot on the Morning of June 17, 1996 27
Figure 13. Langley Plot with LMS on Morning of June 17, 1996 28
Figure 14. Direct Irradiance on October 23, 1996 29
Figure 15. Langley Plot on Afternoon of October 23, 1996 30
Figure 16. Histogram of all AOD 32
Figure 17. Monthly Median for all Facilities 35
Figure 18. Monthly Box and Whisker Plot for EF-1 36
Figure 19. Monthly Box and Whisker Plot for EF-3 37
Figure 20. Monthly Box and Whisker Plot for EF-13 38
Figure 21. Monthly Box and Whisker Plot for EF-20 39
Figure 22. Monthly Box and Whisker Plot for EF-24 40
Figure 23. Daily Box and Whisker Plot for March 1997 at EF-13 42
Figure 24. 20-Second AOD Values for the Morning of October 26, 1996 at EF-13 43
Figure 25. IQR of AOD for Morning of March 5, 1997 at All Facilities 46
FigureA1. Airmass for Angles 0° to 90° 57

LIST OF ABBREVIATIONS

AOD	Aerosol Optical Depth
ARM	Atmospheric Radiation Measurement program
CART	Cloud and Radiation Testbed
CMDL	Climate Monitoring and Diagnostics Laboratory
DOE	Department of Energy
DU	Dobson Units
EF	Extended Facility
GCM	Global Climate Model(s)
GMT	Greenwich Mean Time
IQR	Inter Quartile Range
kPa	1000 Pascal
LMS	Least Median Squares
MFRSR	Multi-Filter Rotating Shadowband Radiometer
nm	Nanometer
NOAA	National Oceanic and Atmospheric Administration
O3OD	Ozone Optical Depth
ORNL	Oak Ridge National Laboratory
PCA	Principal Components Analysis
PM	Particulate Matter
PM_{10}	Particulate Matter with a diameter less than or equal to 10 microns
$PM_{2.5}$	Particulate Matter with a diameter less than or equal to 2.5 microns
ROD	Rayleigh Optical Depth
SGP	Southern Great Plains
SMOS	Surface Meteorological Observation System
TOA	Top Of Atmosphere
TOD	Total Optical Depth

1. INTRODUCTION

Aerosols are small particles that are suspended in the atmosphere. The stead state concentration of these particles in the atmosphere is on the rise as humans create more of them everyday. There are many anthropogenic sources, both urban and rural, including factories, open burning, farming and automobiles. There are also natural sources of atmospheric aerosols, such as volcanoes. New environmental regulations have been promulgated for the particulate matter in the lower atmosphere smaller than or equal to 2.5 micrometers ($PM_{2.5}$) in diameter in the last year. The issues of concern that prompted the new regulations were the threat of $PM_{2.5}$ to the health of the human respiratory system and visibility reduction by the fine particles. Another concern is the impact of aerosols on global warming. Currently society and science are scrutinizing the local, regional and global effects of aerosols in the Earth's atmosphere, yet their variability within time and space is not well known.

In July 1997, the EPA issued new Particulate Matter (PM) standards under the National Ambient Air Quality Standards[1]. This update added new $PM_{2.5}$ annual and 24-hour standards, while revising the 24-hour PM_{10} standard. These revisions were based on reports of the serious health hazards that the fine particulate matter poses. The PM is a physical measurement of the aerosols found in the breathing zone of our atmosphere near the surface. These new regulations deal with lower atmosphere aerosols on local and regional levels.

The issue of global warming had recently held the attention of world leaders and scientists with the signing of the Kyoto Accord in December of 1997. In the Accord many nations agreed to reduce anthorpogenic emissions of six "greenhouse gases" to the atmosphere because of global warming predictions by Global Climate Models (GCMs). GCMs divide the Earth's surface into large regions referred to as grids for calculations. Grids vary in size dependent upon the specific model and latitude. GCMs assume that some grid or sub-grid processes are homogenous, and the models represent those process states using one average number. Many of the input parameters to the GCMs, like cloud cover, ozone concentration, water vapor, and aerosol loading, vary on a scale that is much smaller than a GCM grid. More complex models, working on a more detailed spatial scale, are needed to better predict the long-term changes of the global climate[2]. While research is needed to improve these models, accurate measurements are imperative to the models. The Atmospheric Radiation Measurement (ARM) program, sponsored by the Department of Energy (DOE), has committed to collect, document, and archive data critical to GCM research over a long time period (20 years)[3].

The atmospheric column aerosol loading, as represented by aerosol optical depth (AOD) is one of the inputs to GCMs and radiative transfer models of interest. Whole atmosphere aerosol concentrations play a critical role in affecting cloud formation and altering atmospheric radiative transfer[4]. These are two of the important processes, affecting surface temperature and precipitation. AOD has been shown to be one of the most important parameters in many radiative transfer models. Literature[5] indicates local

variations of 13.5 W/m^2 of the direct-normal solar irradiance would result from a change in the AOD value of 0.01. The sensitivity of atmosphere radiative calculations to other model parameters such as precipitable water and ozone was found to be smaller by an order of magnitude when compared to aerosols under clear-sky conditions.

The influence of aerosols to climate prediction is one area of interest to ARM's ongoing multi-year experiments. To improve GCMs and parameterize aerosol processes the spatial and temporal variations of AOD needs to be thoroughly characterized. The AOD used in radiative transfer calculation has typically been taken as a constant for a GCM grid[6]. To explore the spatial and temporal variation of AOD and its impacts on the GCM predictions, surface radiometric data from five facilities at the ARM Southern Great Plains (SGP) Cloud and Radiation Testbed (CART) Site was analyzed. The radiometric data from 1 May 1996 to 31 April 1997 were retrieved from the ARM archive[7] located at the Oak Ridge National Laboratory (ORNL) in Oak Ridge, Tennessee. The AOD values at five facilities at the SGP site were then calculated and analyzed using the Least Median Squares-Langley (LMS-Langley) technique developed at ORNL[8] and described in the Theory and Methodology section.

2. DESCRIPTION OF SITE AND DATA

The CART site shown in Figure 1 was designed to observe and provide needed data for the improvement of GCM prediction and cloud parameterization. The site was about the size of a mid-latitude GCM grid, approximately 250 km (155 miles) (East to West) by 350 km (218 miles) (North to South) and was centered at Lamont, Oklahoma. The elevation varied from 217 to 664 meters above sea level and covered the area between 99.3 to 95.5°W latitude and 38.3 to 34.8°N longitude.. The primary land use at the site was agricultural, either cropland or pasture. No significantly large pollution sources were nearby; thus it was believed to be representative of a rural continental site. Hundreds of meteorological instruments were installed at the CART site. More than 4 million geophysical variables have been collected each day; the sampling intervals range from seconds to minutes[9].

This study focused on five extended facilities (EF) that housed the Multi-Filter Rotating Shadowband Radiometers (MFRSR). These facilities are denoted as, EF-1, EF-3, EF-13, EF-20, & EF-24 on the figure. They are located at the four corners (EF-1, EF-3, EF-20 and EF-24) and the center (EF-13) of the CART site for maximum spatial coverage. The MFRSR was phased into use in 1994 to gather shortwave spectral solar radiation data at the CART site. The MFRSR, as shown in Figure 2, measured diffused horizontal and total horizontal solar irradiance at 20-second intervals. The MFRSR took a series of four measurements in each pass. The first was with the shadowband at nadir and measures

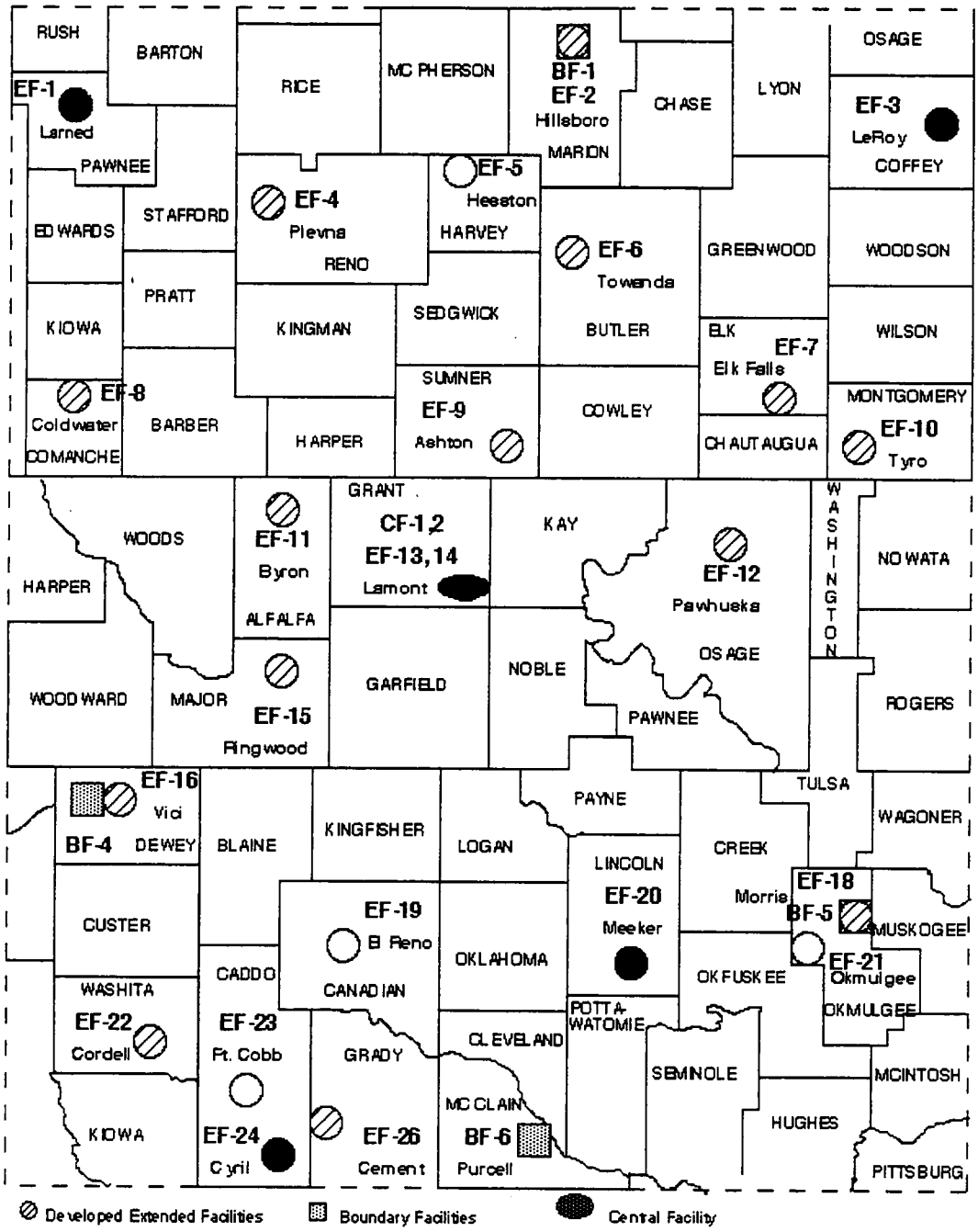

Figure 1. Map of ARM SGP CART Site with Facilities of Interest as Solid Circles (scale: 50km/in)

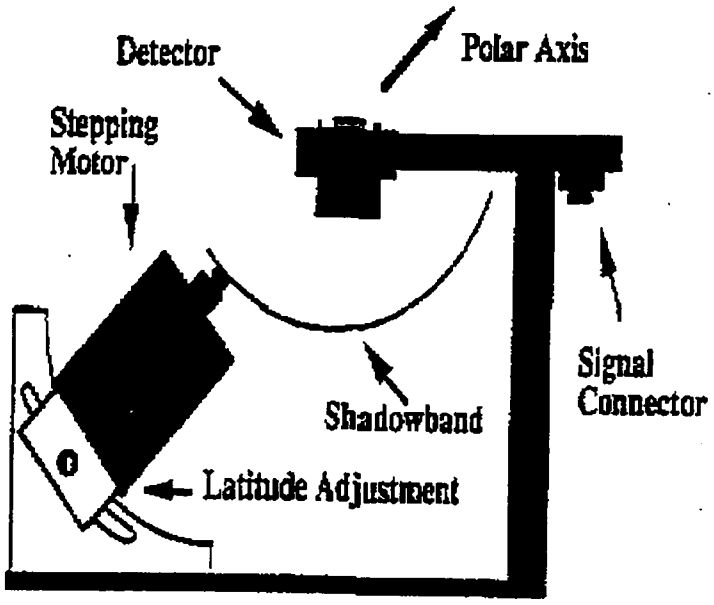

Figure 2. The Multi-Filter Rotating Shadowband Radiometer
Source: http://www.arm.gov/docs/documents/technical/conf_9303/2670a_10/michalsky_3/figure_1.html

total horizontal solar irradiance. The next three measurements were with the band at 9° to one side of the sun, then directly blocking the sun, and then 9° to the other side. The diffused horizontal irradiance was measured when the shadowband was blocking the sun, but because the band is larger than the solar disk, corrections had to be made. The two measurements at 9° were taken to correct for the extra width of the shadowband. The direct normal narrowband irradiance was the difference between the total and corrected diffused solar irradiance[10]. The central wavelengths for these narrowband measurements were 415, 500, 608, 664 and 860 nanometers (nm) and they had a 10 nm full width at half maximum. In this analysis, the direct normal narrowband irradiance of these five wavelengths was used for the AOD calculations, with a focus on 500nm. Figure 3 shows an example of the direct normal-narrowband irradiance on January 28, 1997, a clear-sky day at five wavelengths, with the maximum at local noon and minimums at sunrise and sunset. The shape shown here is characteristic for direct solar irradiance at each specific wavelength. Figure 4 is similar but March 2, 1997 has some cloudy periods. Note how the basic shape of the irradiance curve was retained by the less or non-cloudy portions of the day. The AOD was derived for these five (5) wavelengths from the MFRSR data using the LMS-Langley technique[8].

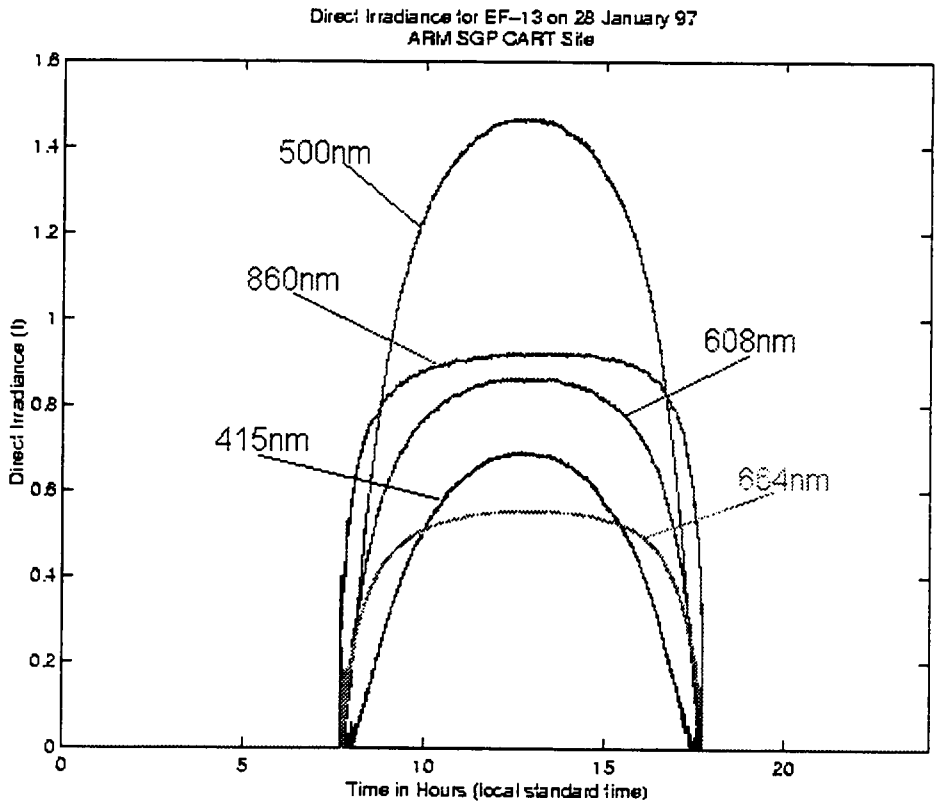

Figure 3. Example of Direct Normal Narrowband Irradiance with Clear Skies

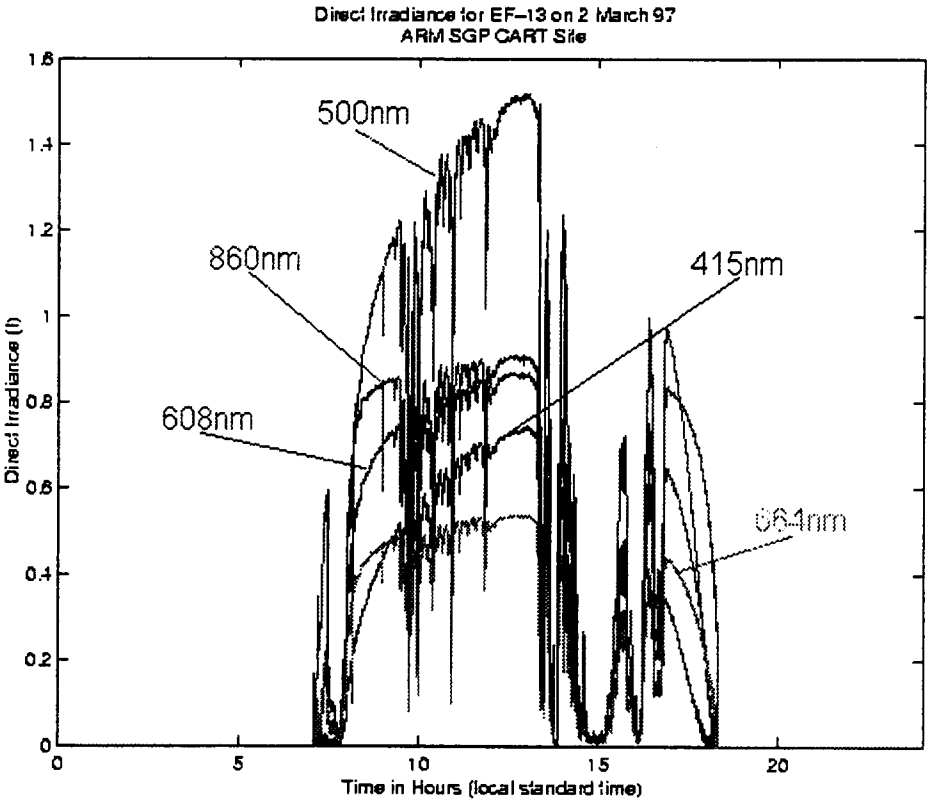

Figure 4. Example of Direct Normal Narrowband Irradiance with Cloudy Skies

3. THEORY AND METHODOLOGY

The AOD is a fraction of the total optical depth (TOD). The TOD is the extinction coefficient for solar irradiance that is scattered or absorbed by all material in the MFRSR viewpath as it passes through the Earth's atmosphere. The majority of the materials in this viewpath includes aerosols, air molecules, ozone, water vapor, clouds and trace gases. When calculating the clear-sky AOD, corrections were required for the Rayleigh scattering by air molecules, ozone absorption, and water vapor absorption. At the wavelengths considered, absorption and scattering of light by water vapor and trace gases were insignificant, thus the correction for these were not performed. Since only the clear-sky effects of aerosols on radiative transfer was of interest, the cloudy periods were removed after the LMS regression was performed. The TOD is the linear sum of the AOD, Rayleigh scattering, and ozone absorption[4].

Equation 1. The components of Total Optical Depth (TOD)

$$TOD = AOD + ROD + O3OD$$

where:

TOD = Total Optical Depth (unitless)

AOD = Aerosol Optical Depth (unitless)

ROD = Rayleigh Optical Depth (unitless)

O3OD = Ozone Optical Depth (unitless)

Total Optical Depth (TOD)

TOD was computed by the Langley method described by Cheng, et. al.[8] that used the robust LMS regression technique. The Langley Law describes the attenuation of solar irradiance as it passes through the atmosphere.

Equation 2. The Langley Law for one wavelength

$$I = I_o e^{-\tau m}$$

where:

I = Spectral irradiance at the ground surface (W m^{-2})

I_o = Spectral irradiance at the top of the atmosphere (W m^{-2})

m = Airmass (unitless)

τ = Total optical depth (unitless)

I is the direct normal irradiance measurement from the MFRSR. The airmass is the ratio between the slant optical path of light through the atmosphere and the vertical optical length. Figure 5 shows that the distance through the atmosphere that the light must travel is dependent upon the angle light enters the atmosphere. The ratio of the vertical path to the actual path length through the atmosphere produces a unitless length referred to as airmass[11]. When the sun is directly overhead (perpendicular to the Earth's surface), airmass (m) is one. Airmass was calculated from Equation 3 derived by Kasten's [12] using the relative position between the Earth and the Sun; i.e. the day of the year and time of day (or angle to the sun). At large angles, above 85°, this approximation is not valid. Figure A1 in the Appendix illustrates the airmass found at zenith angles from 0° to 90°.

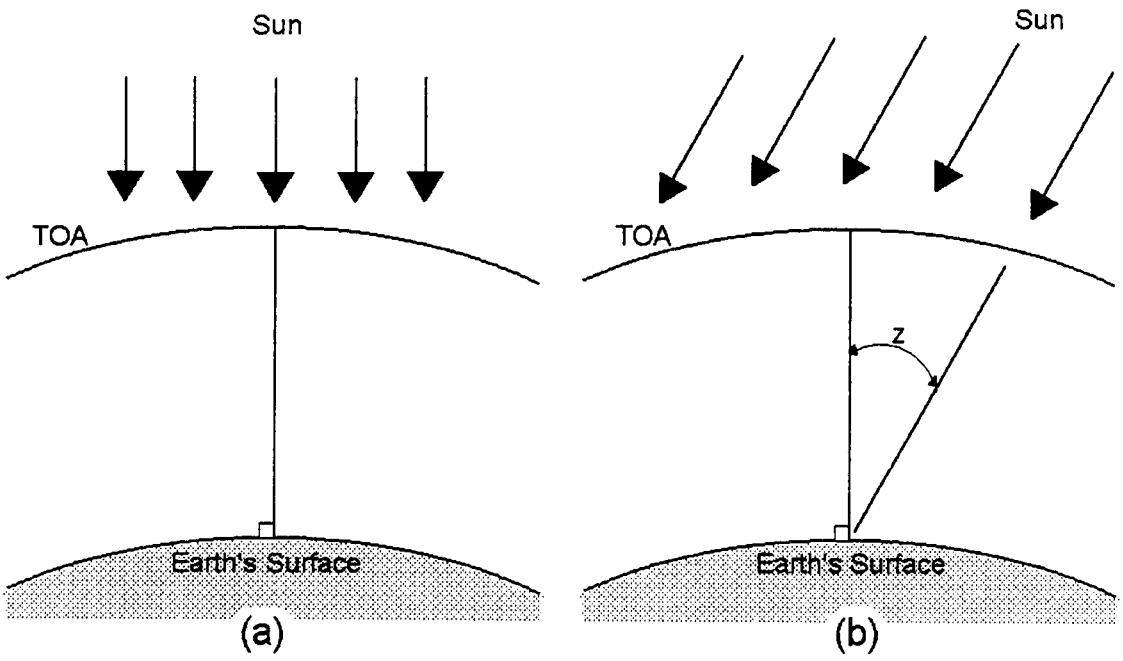

Figure 5. Light travel through the Atmosphere

Equation 3. Airmass

$$m = \frac{1}{\cos(z) + 0.15 * e^{\left\{-1.253*\log\left[93.885-\left(z/0.01745329\right)\right]\right\}}}$$

where:

z = Zenith angle in radians

The TOD or τ is the extinction coefficient for the loss of intensity in the spectral irradiance as it passes through the atmosphere. This loss of intensity is due to the scattering and absorption of irradiance by materials present in the atmospheric column. The TOD is the atmospheric light extinction normalized to a unit atmosphere[13].

Equation 4. The Natural Log of the Langley Law

$$\ln(I) = \ln(I_o) - \tau m$$

This form of Equation 2 allows a linear regression to be performed to best fit a straight line for extrapolation back to an airmass (m) of zero. At an airmass of zero (top of the atmosphere), the $\ln(I)$ value found is $\ln(I_o)$. The LMS minimizes the median squared residual from the regression analysis[14]. LMS is very robust to outliers and has a breakdown point of 50%. The objective of using LMS was to find a line that fits the majority of the data and then those data points that were identified as outliers were removed. For acceptance of the regression line the R^2 value for the best fit must be 0.95 or higher in the LMS-Langley algorithm. I_o was computed for morning and afternoon periods that had an airmass between 2 and 6. At a lower airmass the "rate of change of

the air mass is small, creating a greater opportunity for changing atmospheric conditions to affect the regression"[15]. There is also uncertainty in the larger airmasses due to " refraction corrections that are increasingly sensitive to atmospheric temperature profiles"[15]. Airmass restrictions are used when performing a LMS regression analysis on Equation 4.

Rayleigh Optical Depth (ROD)

Rayleigh Optical Depth (ROD) is the amount of light that is scattered or absorbed in the atmosphere by the molecules of air as the light travels to the surface. There are many empirical equations available from the literature[16] for calculating the ROD. Equation 5 from Hansen and Travis was chosen so that comparisons could be made with the work of others[15].

Equation 5. Rayleigh Optical Depth equation used[16, 17].

$$ROD=0.008569 * \lambda^{-4} (1+0.0113*\lambda^{-2} +0.00013*\lambda^{-4})$$

where:

λ = Wavelength in nm

ROD = Rayleigh Optical Depth (unitless)

This equation is for sea level so correction is needed for the change in atmospheric pressure at each facility by multiplying the ROD by the actual barometric pressure and dividing by the pressure at standard conditions (101.325 mbars). The actual barometric pressure at 1 meter height was taken at each ARM facility by the Surface Meteorological

Observation System (SMOS)[18] in 30 minute intervals. The magnitude of ROD is inversely related to the wavelength. As the wavelength increases the amount of solar irradiance that is scattered by molecules decreases.

Ozone Optical Depth (O3OD)

Ozone Optical Depth (O3OD) is the amount of light that is absorbed in the atmosphere by ozone as the light travels to the surface. The ozone concentration of the whole atmosphere was measured by an ozone spectrophotometer at the NOAA/CMDL (National Oceanic and Atmospheric Administration / Climate Monitoring & Diagnostics Laboratory) facility in Nashville, TN. The atmospheric ozone is measured in Dobson Units (DU)[19]. (If all the ozone in a column of air is compressed at standard temperature and pressure (0°C and 1 atmosphere) a 3mm slab corresponds to 300 DU. [20]) The measurement of total atmosphere ozone is dominated by upper atmosphere ozone levels not surface levels. The peak of surface ozone usually occurs in the warm summer months of July, August and September. The DU measurements of total atmosphere ozone peaks in the months of February, March and April. These values were used as they were readily available and there was good agreement with the column ozone abundance estimated at the CART site by other methods[21]. To calculate O3OD, the ozone absorption cross-section from Shettle and Anderson[22] was used to calculate optical depth as shown in Equation 6.

Equation 6. Ozone Optical Depth

$$O3OD = O_3 * X\text{-}SAC * Loschmidt\ \# * Conversion\ Factor$$

where:

O_3 = Ozone measurement from Nashville, TN in Dobson Units (DU)

X-SAC = X-Section Absorption Coefficient in cm^2/molecule

(wavelength dependent)

Loschmidt # = $2.686763*10^{19}$ molecules/cm^3

Conversion Factor = (0.01mm/DU)*(1cm/10mm) = 0.001 cm/DU

The O3OD has a peak absorption in the Chappuis bands at about 600 nm, so it affects the TOD at 608 nm most. Once the TOD, ROD and O3OD are all calculated the AOD was found using Equation 1.

4. RESULTS AND DISCUSSION

In this section all results are given for the wavelength of 500 nm. Smaller wavelengths have an increasing ROD component and the larger wavelengths have increased ozone interference. Because the effects of ROD and O3OD are minimal at 500 nm, the uncertainties in those measurements were less that at the other wavelengths. Therefore, the 500 nm channel was considered a useful wavelength for AOD retrieval[23]. Extrapolation between wavelengths has not been considered due to scattering variations at different wavelengths due to particle size and vertical distribution of the aerosols.

Some examples of the LMS-Langley analysis are shown in the case studies below. The four days show meteorological conditions that vary from a clear day to completely overcast with thick clouds. The second section then looks at the AOD and its characteristics at the site, including basic statistical analysis of all data points found in the year of analysis, time dependence, and spatial variations.

Case Studies

Example days were examined in detail to show the process of the LMS-Langley analysis. These four days cover a wide range of meteorological conditions to show how the analysis handles typical variations of weather in Oklahoma. The first day that is discussed is a clear sky day. The next day is a cloudy day. The last two days both have clouds, one has a short cloud passage and the other has high thin wispy clouds.

January 28, 1997

On January 28, 1997, the skies at Lamont, OK were clear at the Central Facility (EF-13). The direct irradiance for that day can be found in Figure 6. The shape of the curve is a distinctive trait of irradiance measurements taken in the absence of clouds. The data that was between an airmass of 2 and 6 was analyzed in the morning hours. An airmass below 6 began at 14.51 Greenwich Mean Time (GMT) or 8:30 am local time and the airmass dropped below 2 at 16.96 GMT or 10:58 am local time. The Langley plot, natural log (ln) of the direct irradiance data from this time period plotted against the airmass, is found in Figure 7. This shows the linear relationship of the direct irradiance to the airmass as indicated in the Langley equation (3). The LMS regression was performed on this data to find the irradiance intercept when airmass is zero. This intercept value was the I_o or the direct irradiance at the top of the atmosphere. This data set consisted of 440 data measurements taken at 20-second intervals. Figure 8 is the same as Figure 6 but the LMS calculated data points are included as the thick line on the plot. A few data points were removed by the requirement that the standardized residual after the regression must be less than 2.5 for a point to be considered good for the calculations. After the removal of the points that did not meet that requirement there were 422 valid measurements for subsequent calculations. The mean and median TOD calculated (Equation 4) were identical at 0.195 with an extremely small standard deviation ($6.888*10^{-4}$). Barometric pressure during this time ranged from 100.20 to 100.18 kPa, which corresponds to a ROD of 0.1428 to 0.1432. The ozone measured at Nashville was 312 DU for January 28, 1997. The O3OD calculated from this measurement was 0.0093.

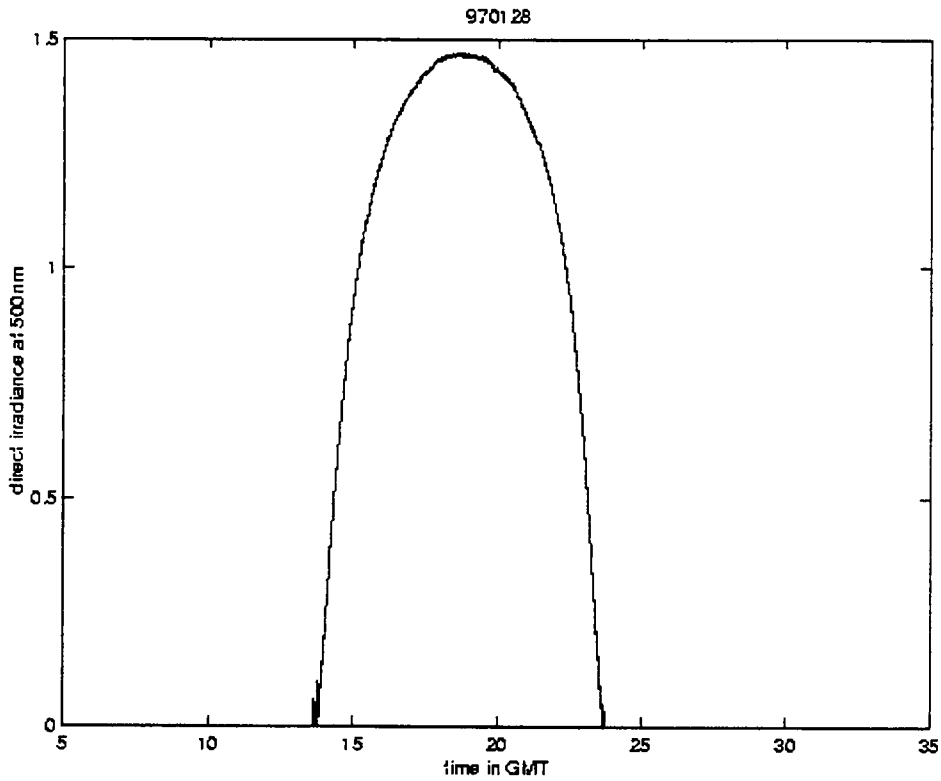

Figure 6. Direct Irradiance on January 28, 1997

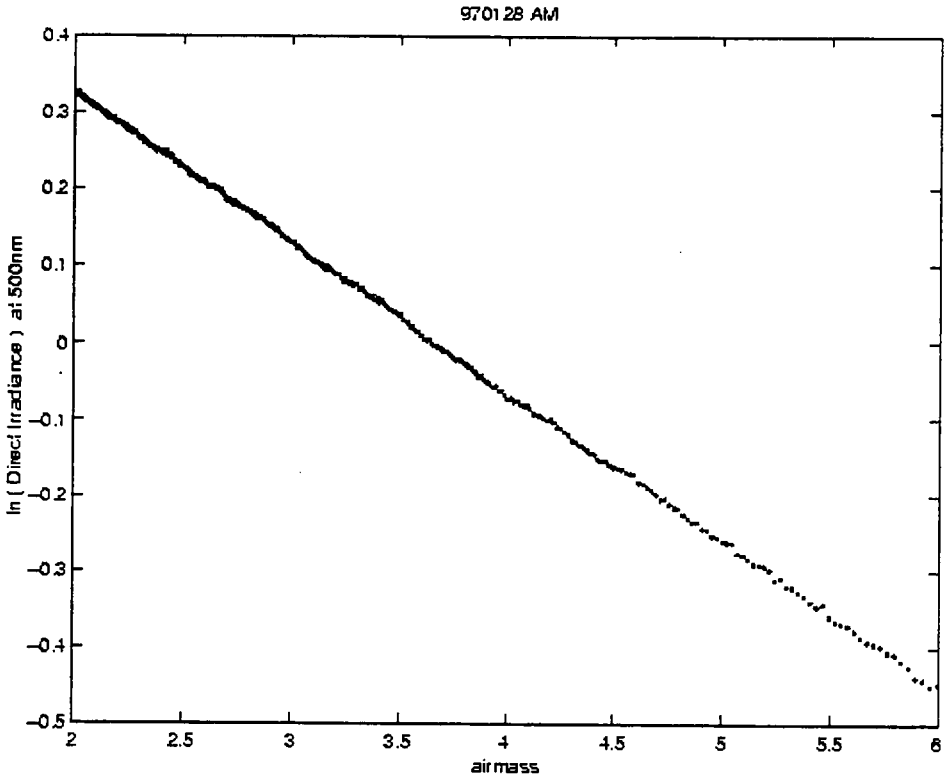

Figure 7. Langley Plot on the Morning of January 28, 1997

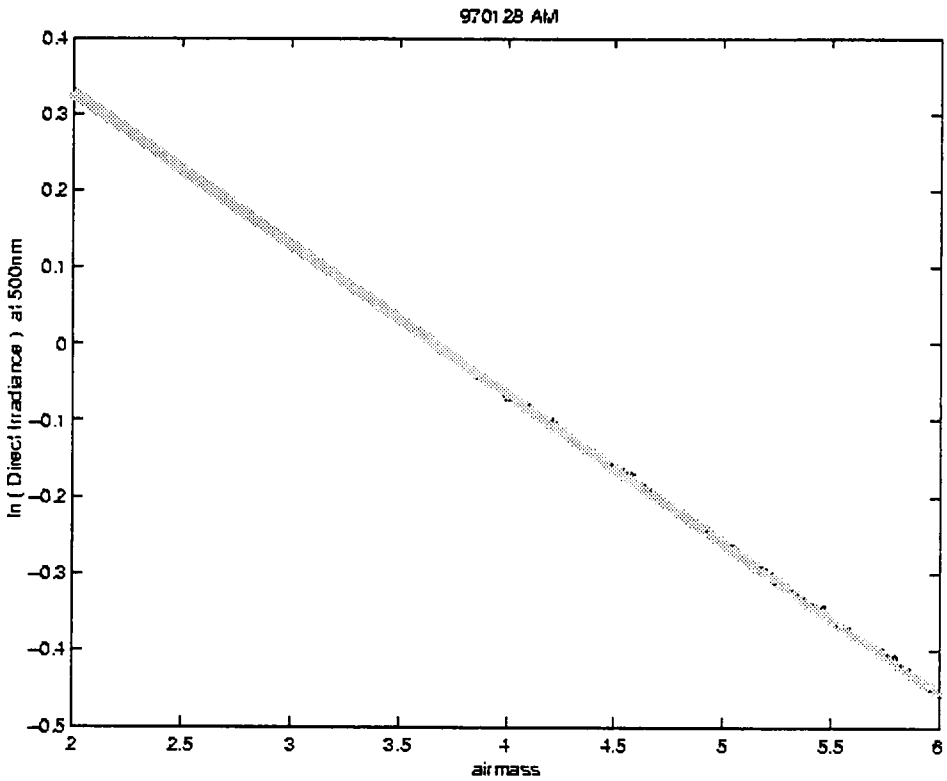

Figure 8. Langley Plot with LMS on the Morning of January 28, 1997

Using equation 1 the calculated AOD for this period of analysis ranged from a minimum of 0.0412 to a maximum of 0.0448 with 0.0430 for the mean and median.

April 3, 1997

Figure 9 shows the direct irradiance found at Lamont, OK on April 3, 1997. Very little direct light passed through the atmosphere to reach the detector. This indicated heavy cloud cover in the viewpath for the day. There was no similarity to the curve as seen on Figure 6 of the clear sky day. In the afternoon most of the measurements of direct irradiance were below detection limits for the MFRSR, meaning the clouds were very heavy. The morning hours saw some limited and infrequent spots of light. Figure 10 shows the Langley plot for the morning of April 3, 1997. There was no indication from this plot of a linear relationship and the LMS algorithm did not produce an answer for this data set. When LMS found no solution, it was an indication that there was no linear relationship. Specifically there was significant cloud passage during the morning hours of April 3, 1997.

June 17, 1996

On June 17, 1996 at Lamont, OK the MFRSR direct irradiance measurements show periods of cloud passing through the viewpath. The direct irradiance can be found in Figure 11. The shape of the curve retains the distinctive curve of direct irradiance with

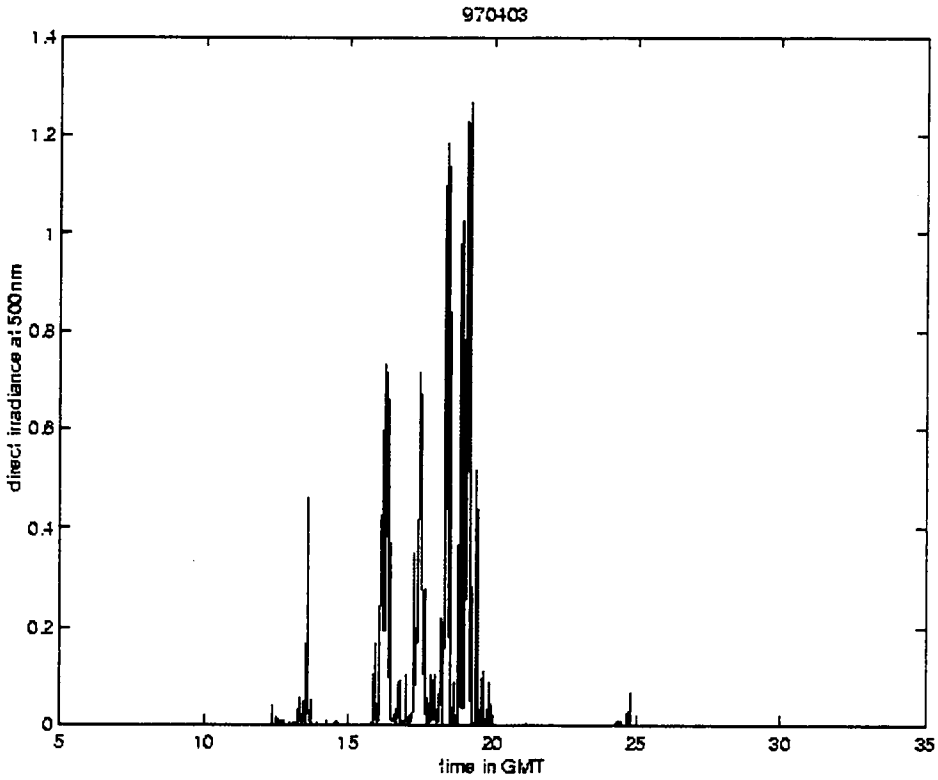

Figure 9. Direct Irradiance on April 3, 1997

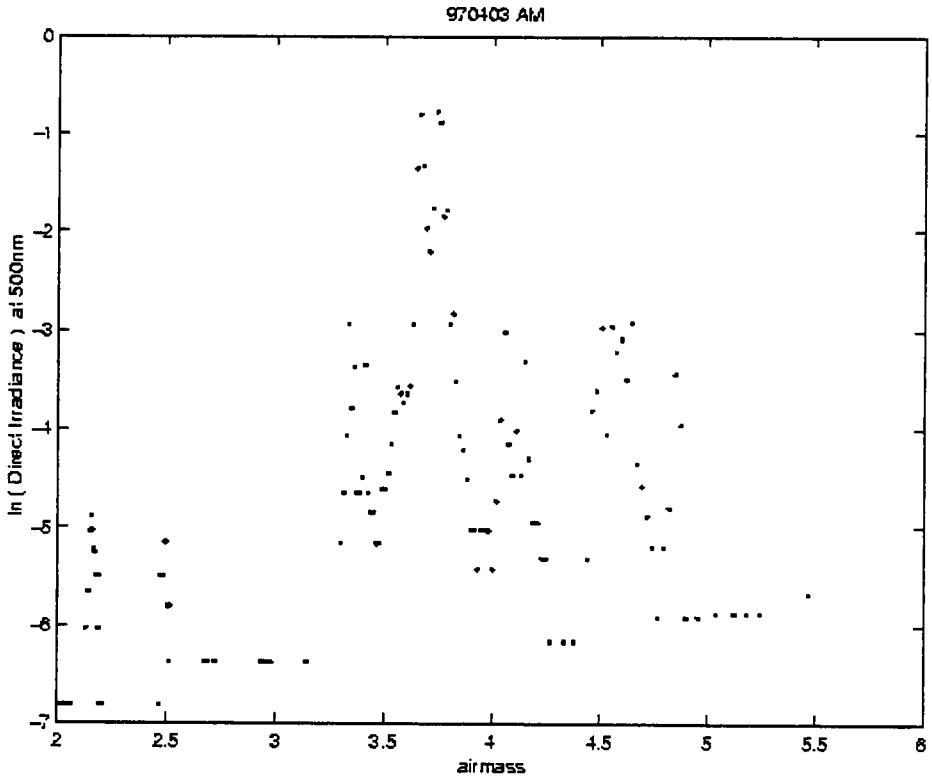

Figure 10. Langley Plot on Morning of April 3, 1997

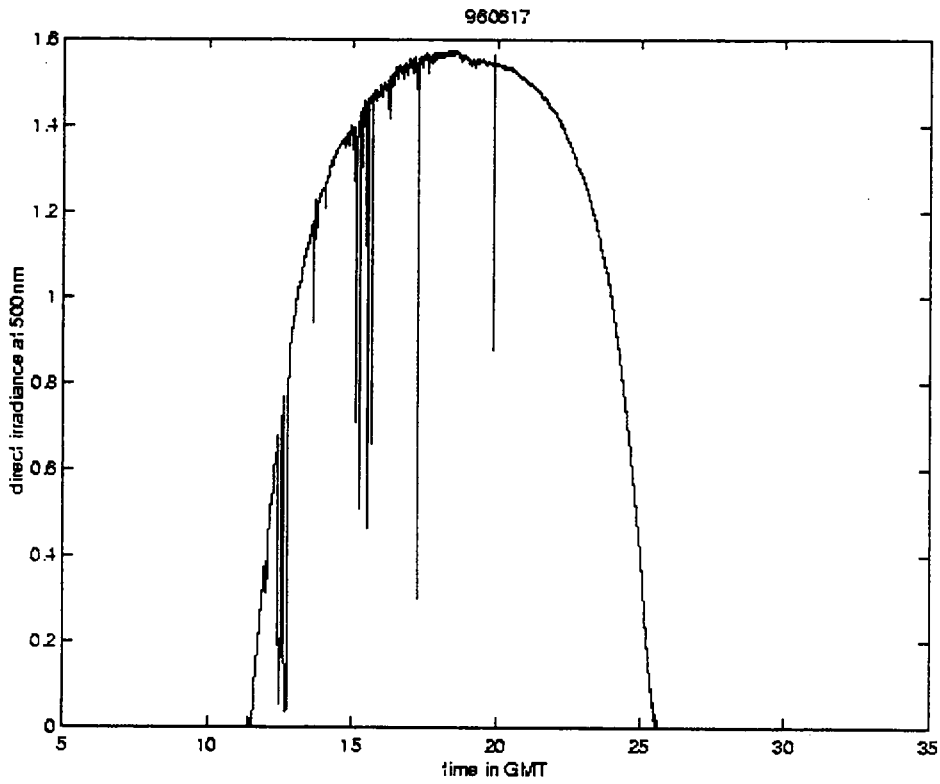

Figure 11. Direct Irradiance on June 17, 1996

the cloud passage as obvious outliers. The airmass entered the range of 2 to 6 at 12.12 GMT (7:07am local time). At 13.89 GMT or 8:53 am (local time) the airmass dropped below 2. The Langley plot is found in Figure 12. Because this day was mostly sunny, the linear trend of the data remains intact. The two obvious deviations from the trend were cloud passages in the MFRSR viewpath. The results of the LMS regression can be found as the open circles on Figure 13. The irradiance measurements that were filtered out by the LMS standardized residual requirement are obviously the clouds that passed through the view path of the MFRSR that morning. Initially 320 measurements were taken in the morning period of analysis; 235 of them met the requirements for the regression analysis and were accepted. The TOD for that period had a mean of 0.256 and a standard deviation of 0.0029. Barometric pressure during this time ranged from 100.20 to 100.25 kPa, which corresponds to a ROD of 0.1395 to 0.1396. The ozone measured at Nashville was 310 DU for June 17, 1996. The O3OD calculated from this measurement was 0.0092. The AOD calculated from Equation 1 had a mean of 0.106 and standard deviation of 0.003.

October 23, 1996

On October 23, 1996, some clouds passed through the MFRSR viewpath. Figure 14 shows the direct irradiance measured for the entire day. The clouds passed overhead in the afternoon hours. Figure 15 shows the Langley plot for the afternoon. There was an indication of a linear trend seen in this figure. The analysis procedure however, rejected

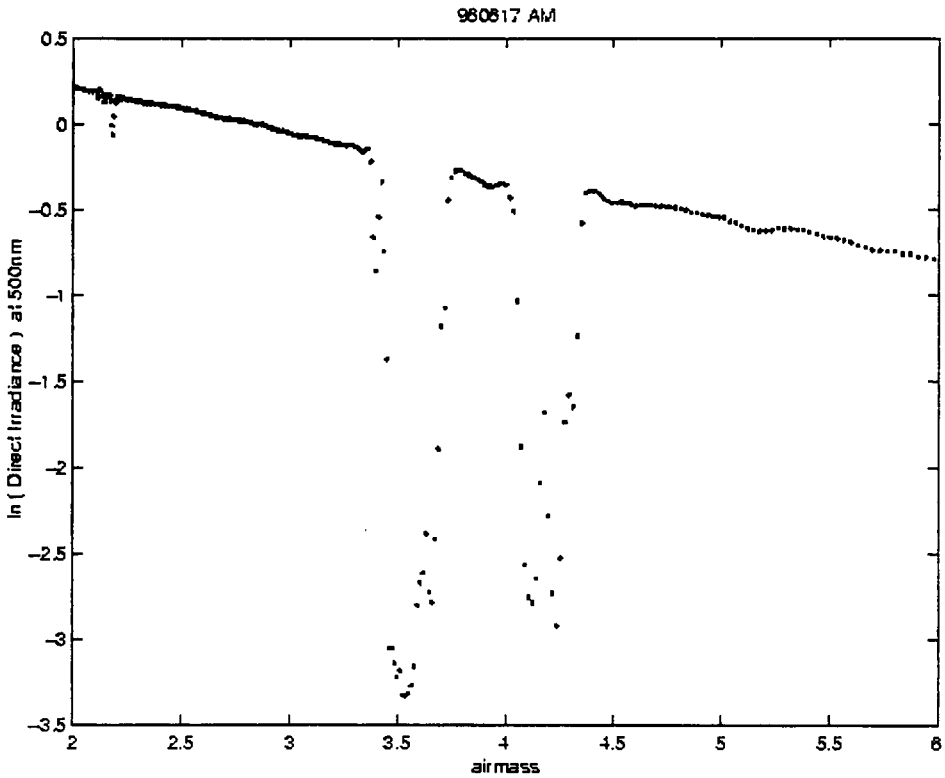

Figure 12. Langley Plot on Morning of June 17, 1996

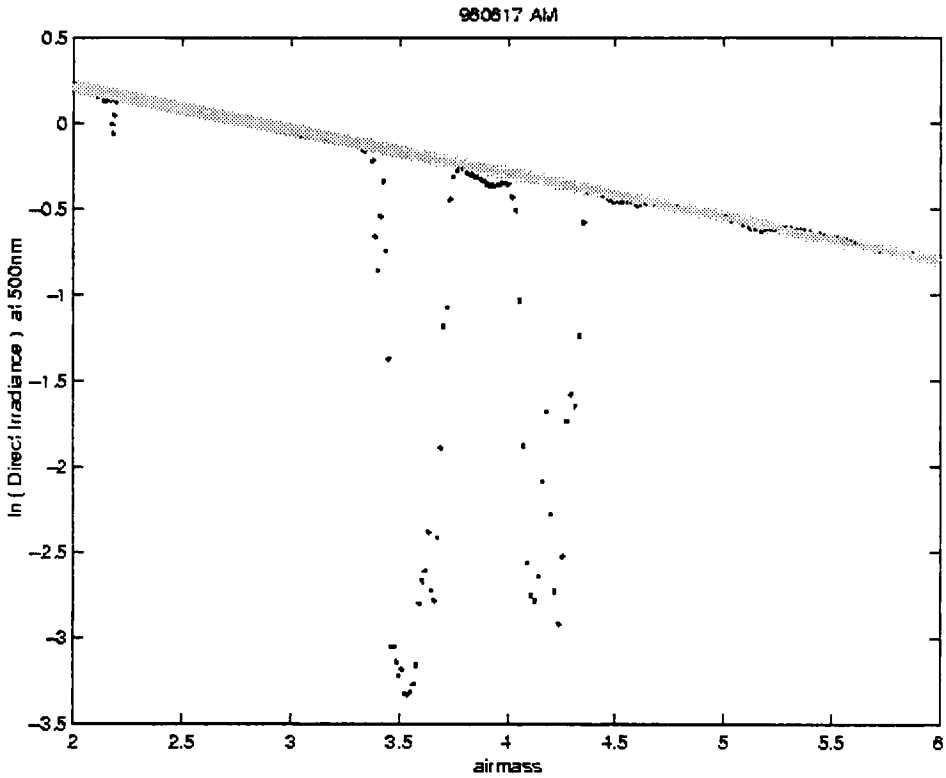

Figure 13. Langley Plot with LMS on Morning of June 17, 1996

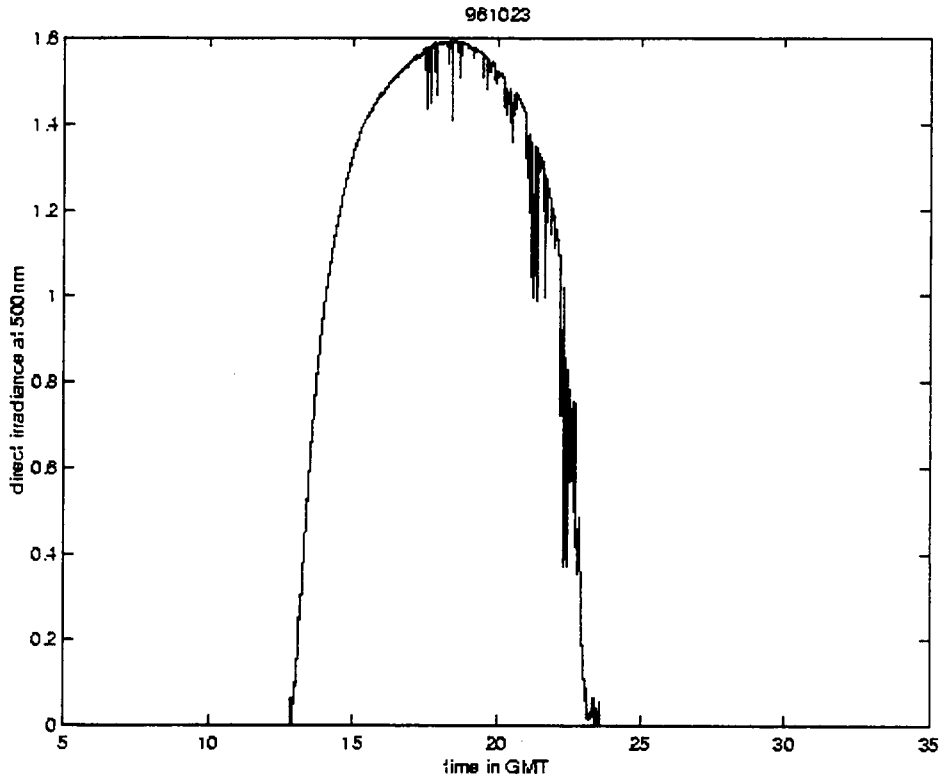

Figure 14. Direct Irradiance on October 23, 1996

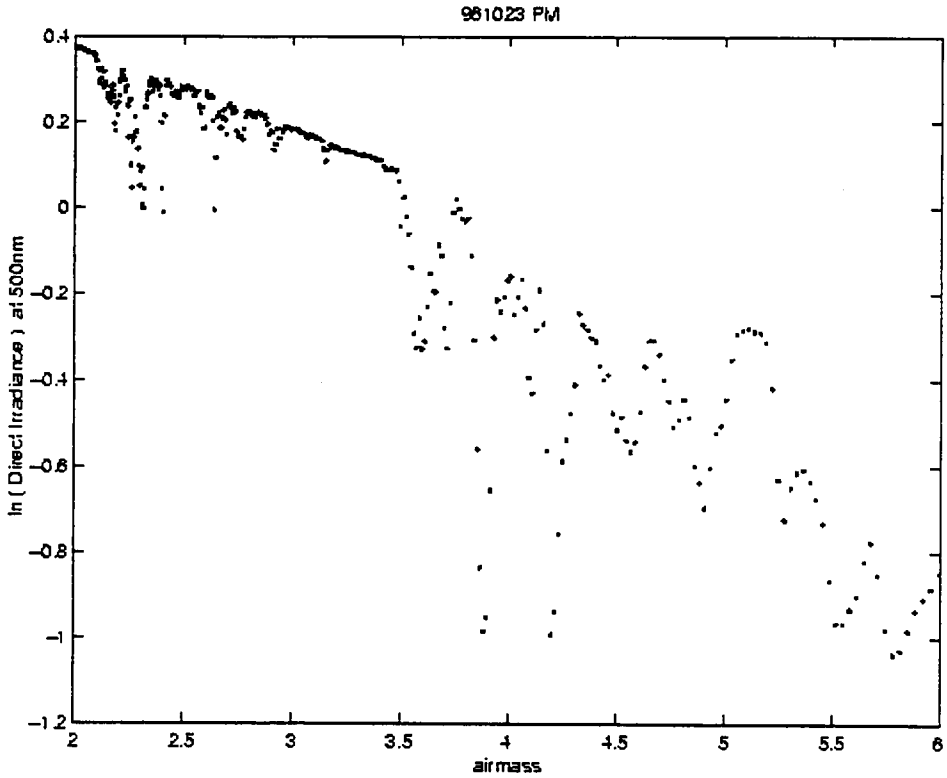

Figure 15. Langley Plot on Afternoon of October 23, 1997

the LMS answer because it did not meet the $R^2 \geq 0.95$ requirement. This means the LMS algorithm did provide an answer but it was not acceptable because it did not describe the linearity of the data to within 95% accuracy. Therefore, all the data for this time period was removed from subsequent analysis.

AOD

There were 532,993 data points from clear skies that were used in the analysis process from the five chosen facilities at the 500 nm wavelength. The basic characteristics of all AOD values found at the SGP CART site were discussed in the following sections. The time dependence of AOD was considered on various time scales. The AOD at the five facilities were also compared to one another for study of spatial variations.

Basic Characteristics of AOD

From the five facilities at the CART site over a half-a-million AOD values were found for the year of analysis. The histogram of AOD values for the entire site is shown in Figure 16. There is a definite concentration of AOD values with a peak in the 0.025 to 0.050 range. Data values of AOD in this range identify clean air masses with little particulate matter in them. The mean value of the AOD from the entire site is 0.129 while the median is 0.086. This indicates a skewed distribution with a thin tail towards the large AOD values. The skewness is computed as 2.5, which confirms what the histogram and mean versus median comparison shows. Standard deviation is 0.132 at the

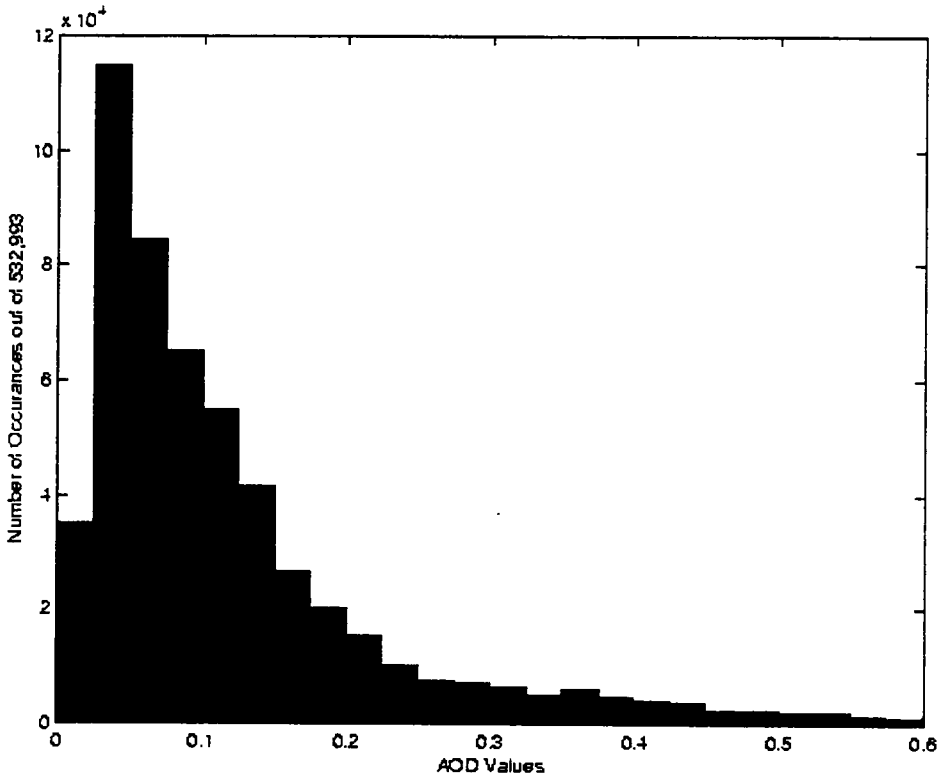

Figure 16. Histogram of all AOD

site. The Inner Quartile Range (IQR) is 0.106 ranging from the 25th percentile of 0.047 to the 75th percentile of 0.153. All of the above information shows the tendency for AOD to be quite small at the SGP CART Site. These small AOD values are expected in a rural area.

Time Dependent Structure

AOD was not at a constant level throughout the year, season, month or even day. To account for the time dependence of AOD each facility has been considered separately. The AOD was found highly variable on all time scales considered; annual, seasonal/monthly, daily, and morning/afternoon.

Annual

Since some distance separates each facility the differences in the year's AOD values is also important to know. In Table 1 the basic statistical description of AOD was shown,

Table 1. AOD by Facility at 500 nm.

Extended Facility	**1**	**3**	**13**	**20**	**24**
# of AOD Values Found	89,556	92,633	122,357	117,609	110,838
Mean	0.078	0.144	0.134	0.153	0.126
Standard Deviation	0.069	0.152	0.124	0.153	0.126
Median	0.056	0.091	0.099	0.104	0.086
25th Percentile	0.034	0.051	0.052	0.057	0.041
75th Percentile	0.104	0.171	0.164	0.176	0.147
IQR	0.070	0.120	0.112	0.119	0.105

separated by facility. The number of AOD values was smallest at EF-1 (89,556) and largest at EF-13 (122,357). It is interesting to note that the two northern facilities (EF-1 & EF-3) had the smaller AOD data sets while the southern three facilities (EF-13, EF-20 & EF-24) had the larger data sets. All variables in Table 1 at EF-1 are smaller than the other facilities. The other facilities had higher mean and median values with larger standard deviations and IQRs. The possible reasons for this difference is discussed in the section on spatial variations.

Seasonal/Monthly

The monthly median AOD values were plotted for all facilities in Figure 17 to show the temporal variations of AOD across the CART site. The minimum in the AOD values occurred in December at four of the five facilities with the smallest median AOD of 0.022 occurring at EF-1. At EF-3 the minimum median AOD of 0.038 was in January. The highest median AOD values were found during the late spring and summer months (May through August). The median summer AOD ranged from 0.130 to 0.354. The pattern of annual AOD variations found at the CART site was similar to those in studies by Smirnov *et. al.*[24] and Devara *et. al.*[25] at other sites. Both studies show minimum AOD values in the winter months and maximum values in the summer. Smirnov *et. al.* reported monthly averaged AOD values from an area in rural Canada that were of the

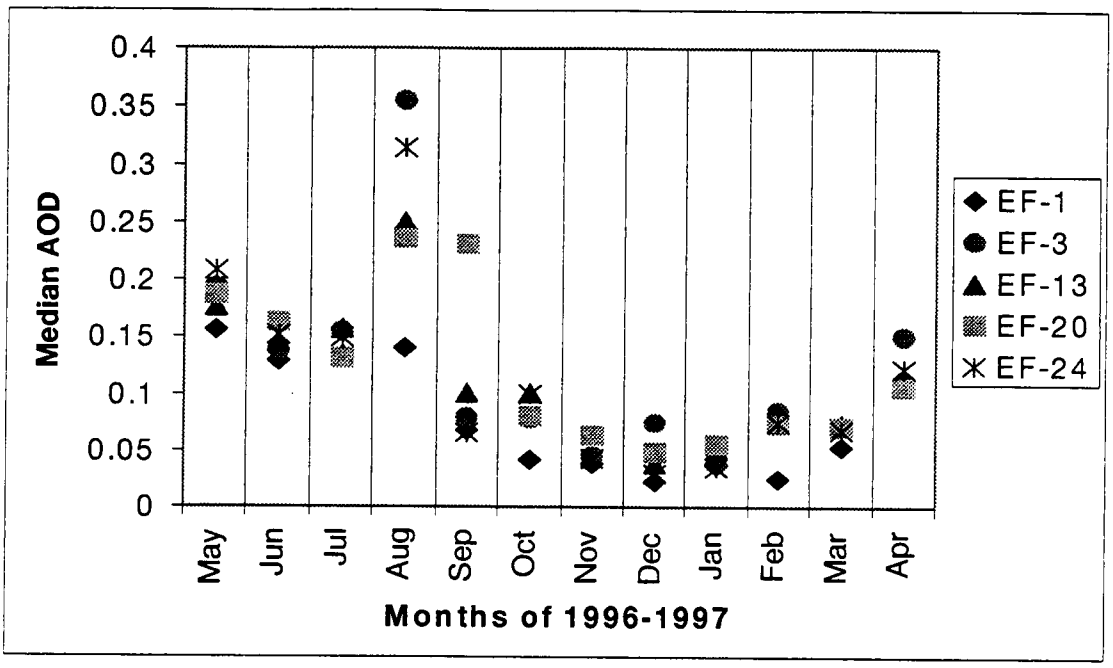

Figure 17. Monthly Median for all Facilities

same magnitude as the ones found at the CART site. While the annual pattern in Figure 17 was similar to Devara *et al.*, their AOD values were much larger than those reported here. The higher AOD values were most likely due to aerosols produced from human activities in the urban area Pune, India.

Figures 18 through 22 show the AOD variations within each month. The maximum IQR of 0.466 occurs at EF-20 (Figure 21) in September. In December at EF-24 (Figure 22), the minimum IRQ of 0.014 is found. There are some similarities in Figures 18 through 22; most notably the IQR for August and September tends to be larger than the other

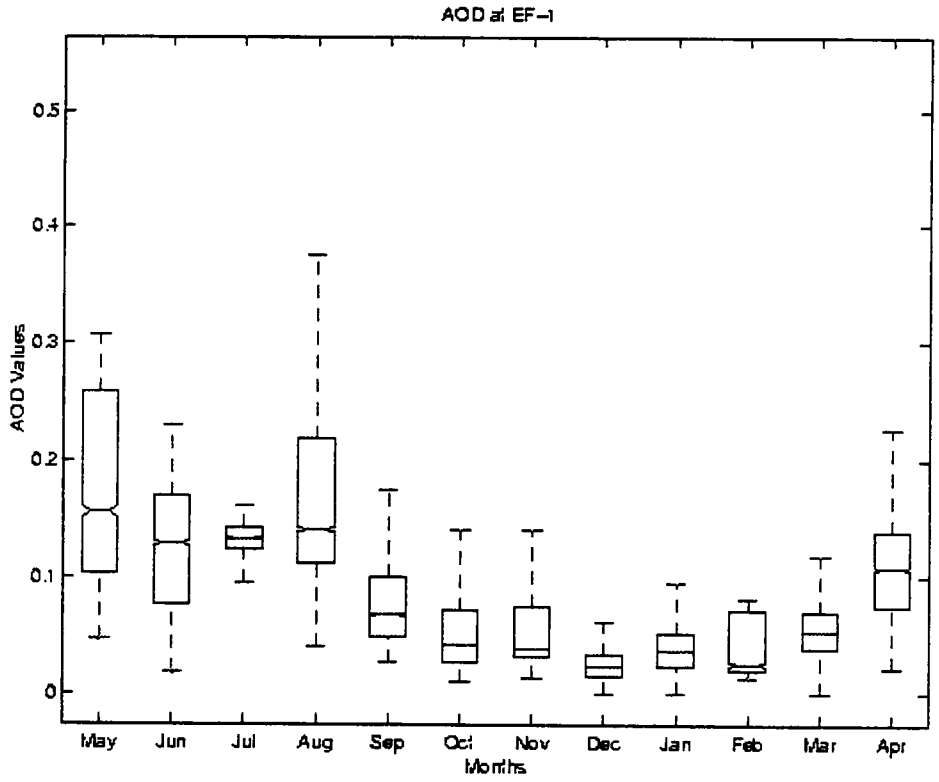

Figure 18. Monthly Box and Whisker Plot for EF-1

Note: The box for each month represents the 25th to 75th percentiles or Inner Quartile Range (IQR) with the center line being the median. The notches around each median are the uncertainty of the median value. The whiskers are 1.5 * the IQR.

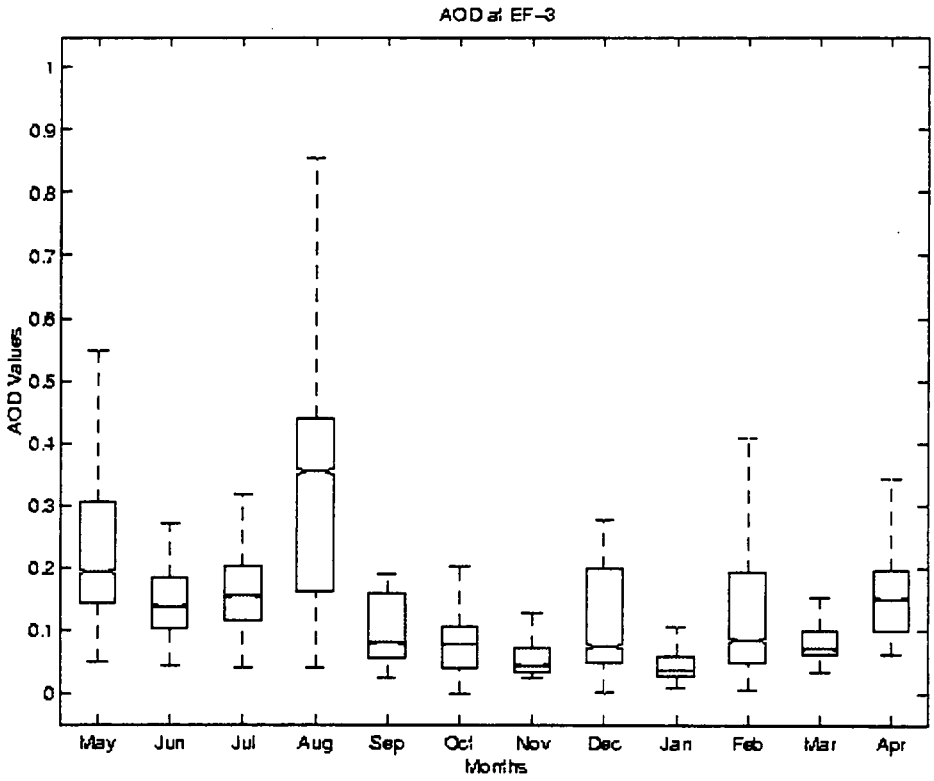

Figure 19. Monthly Box and Whisker Plot for EF-3

Note: The box for each month represents the 25th to 75th percentiles or Inner Quartile Range (IQR) with the center line being the median. The notches around each median are the uncertainty of the median value. The whiskers are 1.5 * the IQR.

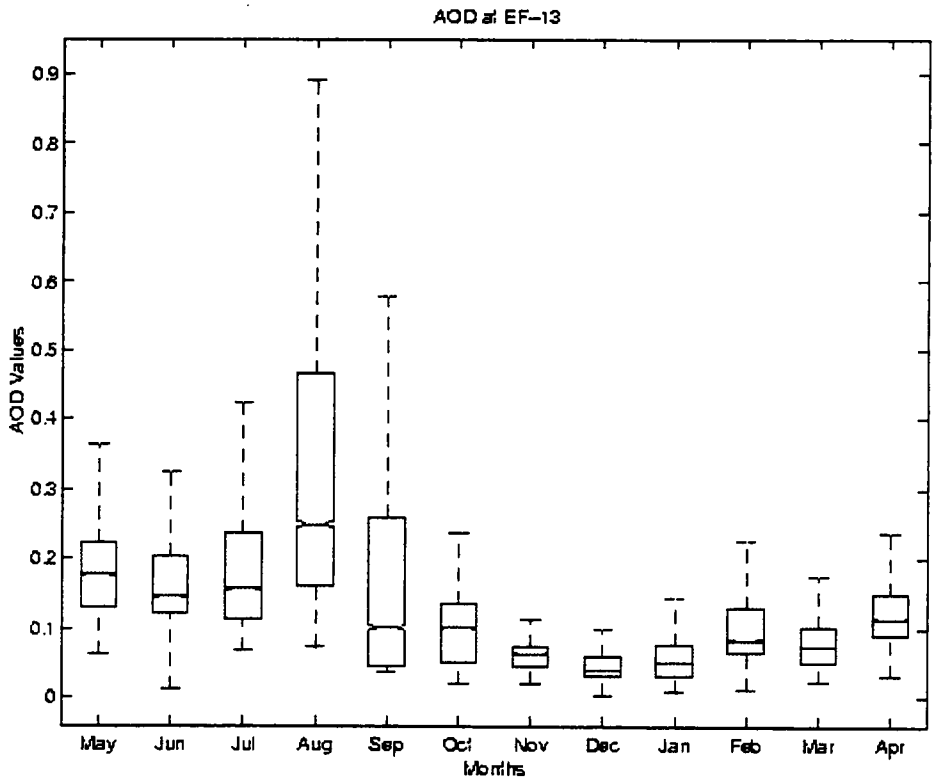

Figure 20. Monthly Box and Whisker Plot for EF-13

Note: The box for each month represents the 25th to 75th percentiles or Inner Quartile Range (IQR) with the center line being the median. The notches around each median are the uncertainty of the median value. The whiskers are 1.5 * the IQR.

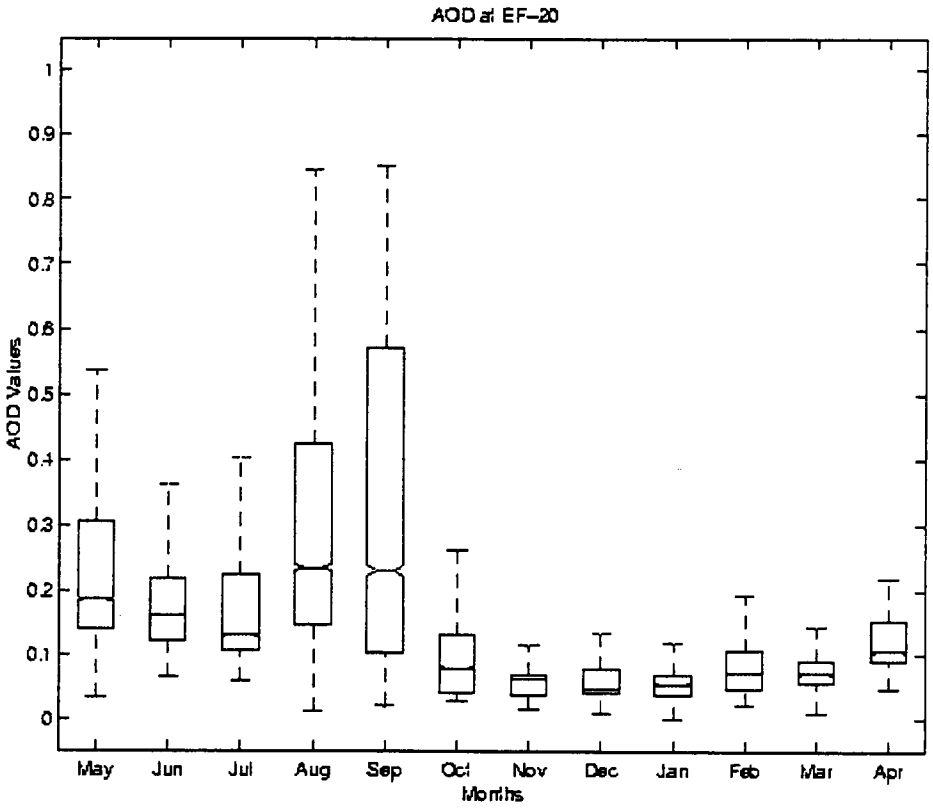

Figure 21. Monthly Box and Whisker Plot for EF-20

Note: The box for each month represents the 25th to 75th percentiles or Inner Quartile Range (IQR) with the center line being the median. The notches around each median are the uncertainty of the median value. The whiskers are 1.5 * the IQR.

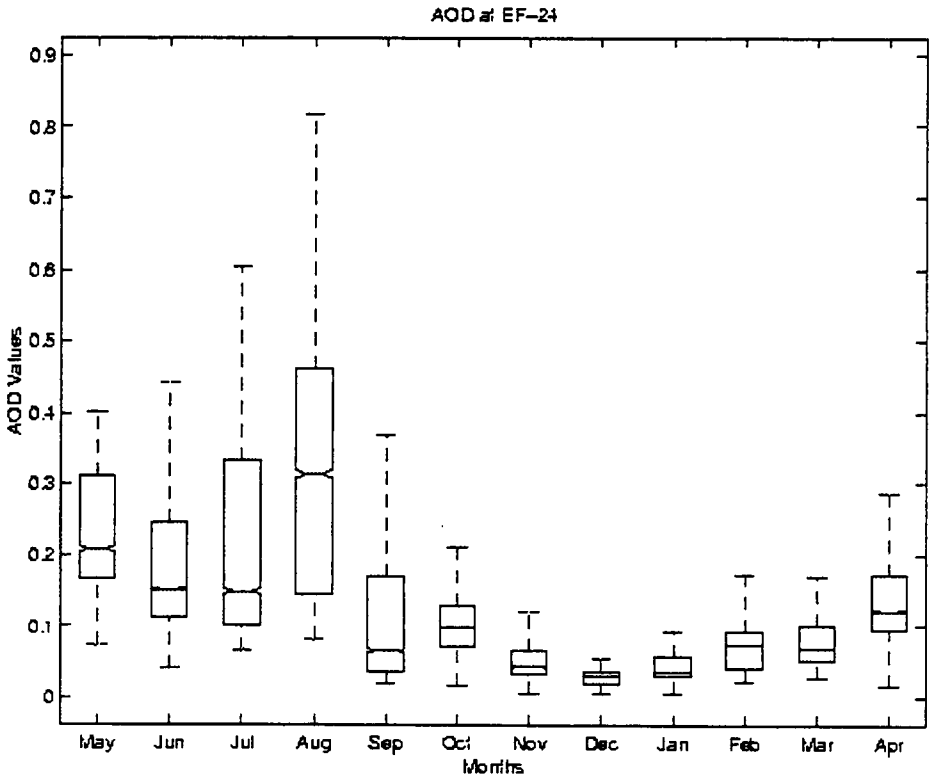

Figure 22. Monthly Box and Whisker Plot for EF-24

Note: The box for each month represents the 25th to 75th percentiles or Inner Quartile Range (IQR) with the center line being the median. The notches around each median are the uncertainty of the median value. The whiskers are 1.5 * the IQR.

months with a few exceptions. During May at EF-1 (Figure 18), there was a larger IQR than any other month at that facility. The other exception is September at EF-3 and EF-24. At these two facilities (Figures19 and 22) there are other months with larger IQR than September but not August. Overall, the months of November, December, January and February had the smallest IQR variations. These fall and winter IQRs range from 0.014 to 0.152. This seasonal variation is typical of the mid-latitudes[26].

Daily Variation

The box and whisker plot in Figure 23 shows the daily AOD values for March, 1997 at EF-13. The 20-second AOD values in March 1997 ranged from a minimum of 0.022 to the maximum of 0.221 with a median of 0.079. The daily variations in Figure 23 show that the magnitude of variations (0.10 min to max) within a single day for AOD is far more than the 0.01 significance levels tested by Hawthore et.al.[5]. For example, on March 28th the IRQ of AOD varies from 0.03 to 0.11. Figure 23 also shows that the AOD can vary substantially from day to day. The AOD on March 21st, 1997 was highly variable from 0.07 to 0.18 (max to min), while on the day before it was only varied from 0.17 to 0.18. Substantial variation of AOD from one day to another was expected, although the number of data points could contribute to the variation.

The 20-second AOD values for the morning of October 26, 1996 at EF-13 were shown in Figure 24. The median AOD was 0.128 with the IQR from 0.125 to 0.130. At about 9:30 local time, there was a local AOD minimum of 0.117. In less than one hour the AOD

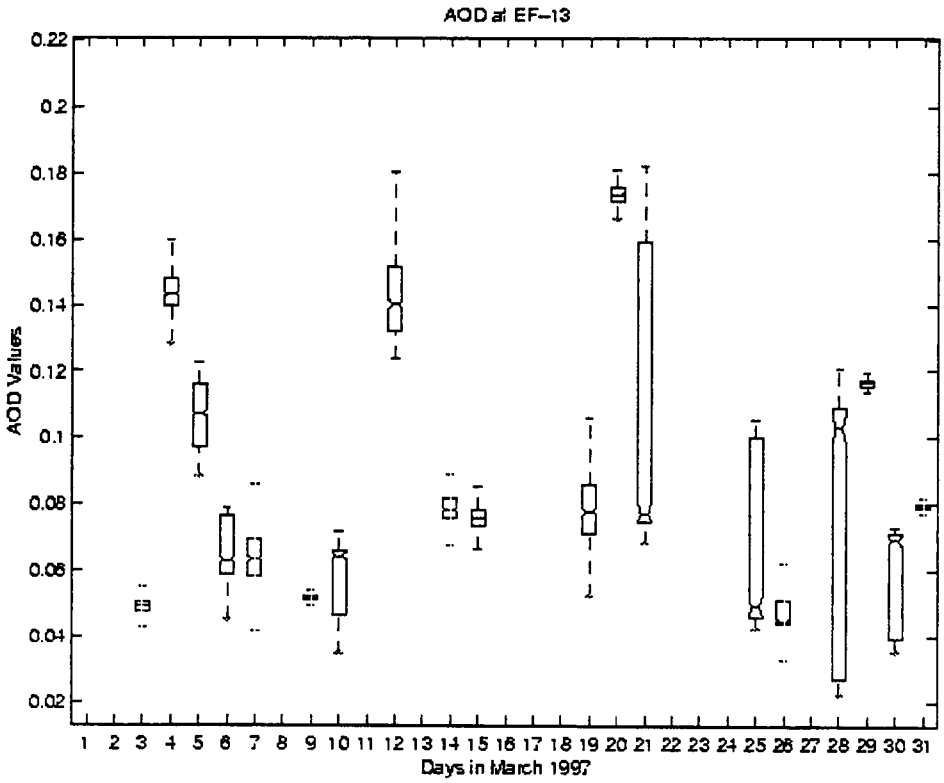

Figure 23. Daily Box and Whisker Plot for March 1997 at EF-13

Note: The median and the 25th to 75th percentiles represented by the box, with the whiskers being 1.5 times the quartile box. The missing days did not meet the LMS-Langley criteria for any significant time frame.

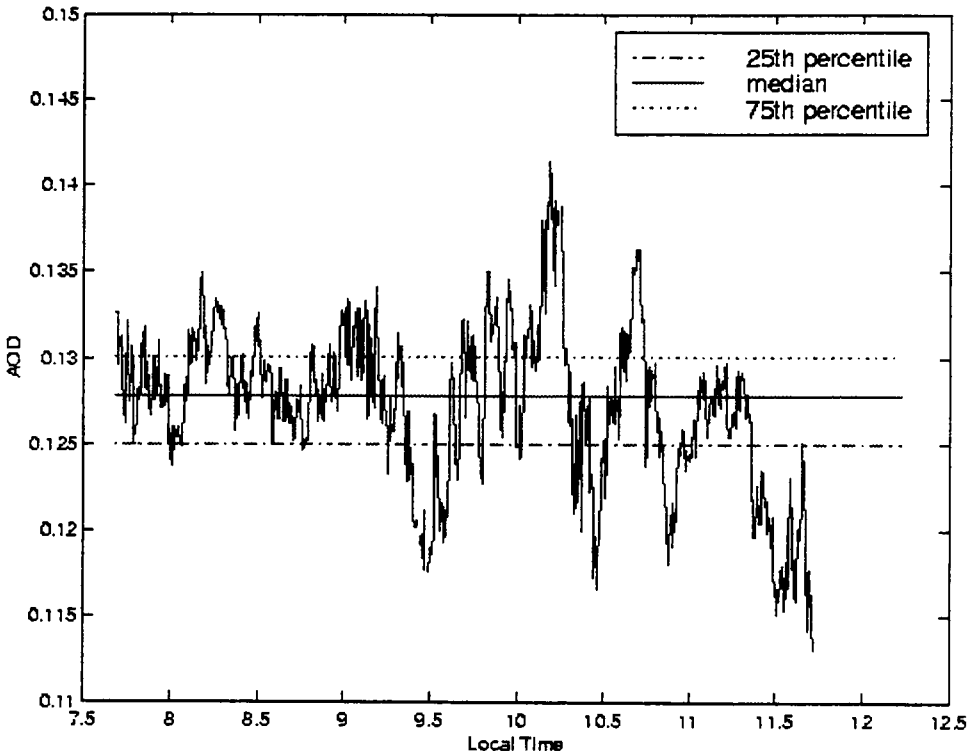

Figure 24. 20-Second AOD values for the morning of October 26, 1996 at EF-13

increased to above 0.140 and then fell to below 0.117. This AOD variation again was substantial.

Morning /Afternoon

AOD values were split into morning and afternoon measurements and then were compared in Table 2. Morning AOD mean and median values were higher than afternoon AOD at all facilities. The percent difference found by subtracting the afternoon value from the morning and dividing that by the afternoon AOD value. To find the percent difference the value found was then multiplied by 100. All percent differences were positive showing that all morning median AOD values were higher than the afternoon values. The morning median AOD was 14% to 58% higher and the mean was 8% to 26% higher than the afternoon AOD median and mean (Table 2). AOD IQR was also higher at

Table 2. Morning versus Afternoon AOD

	E1		E3		E13		E20		E24	
	M	A	M	A	M	A	M	A	M	A
MEDIAN	0.097	0.041	0.099	0.085	0.115	0.097	0.127	0.092	0.124	0.085
MEAN	0.104	0.083	0.149	0.137	0.152	0.127	0.185	0.136	0.154	0.136
IQR	0.111	0.048	0.136	0.111	0.123	0.114	0.151	0.125	0.155	0.104
STD DEV	0.072	0.179	0.141	0.147	0.130	0.097	0.198	0.136	0.122	0.145
% diff. Median	57.9		14.3		15.6		27.3		31.5	
% diff. Mean	19.9		8.4		16.4		26.2		12.1	

all facilities in the morning. The standard deviation was higher in the morning at only two facilities, EF-13 and EF-20. At the three other facilities (EF-1, EF-3, & EF-24), the standard deviation was large in the afternoons.

Spatial Variation

The results thus far demonstrate that AOD varies significantly over time, but how does it vary from place to place? There is very little information on the spatial variation of AOD on a regional scale like the SGP CART site. Studies by Smirnov et al.[24] and Michalsky et al.[26] have considered AOD variation on a scale larger than the CART Site, Canada and the eastern United States, respectively. Alternatively, measurements were taken at only one facility, like Devera et al.[25], but none have considered regional variability of AOD at a facility of the size of the CART site.

The five facilities chosen for analysis were spread out over the CART site to give some insight into AOD variations that occur in space. Initially looking at the whole year mean/median AOD, shown in Table 1, for all facilities there were some differences. EF-1 has much lower mean/median values than that of the other four facilities. This is the first indication that the facilities had differences in AOD due solely to their location. Next considering the box and whisker plots for each facility (Figures 18 through 22), EF-1 again was considerably different from the other facilities. The EF-1 variations were much less that those at the other facilities and AOD values were smaller. Also as noted in the

section on seasonal/monthly temporal variation the IRQ at EF-1 was maximized in May and not August and /or September as it is at the other facilities.

The AOD values could vary significantly from facility to facility. An example of a day with significant variation between the facilities is March 5, 1997. On the morning of that day there was a difference of 0.24 in the median AOD values across the site. EF-1 had a median AOD of 0.06 while EF-20 had a median of 0.31 as seen in Figure 25. This shows that the magnitude of AOD observed at one facility was not necessarily a good indicator of the AOD at other facilities within the SGP CART site.

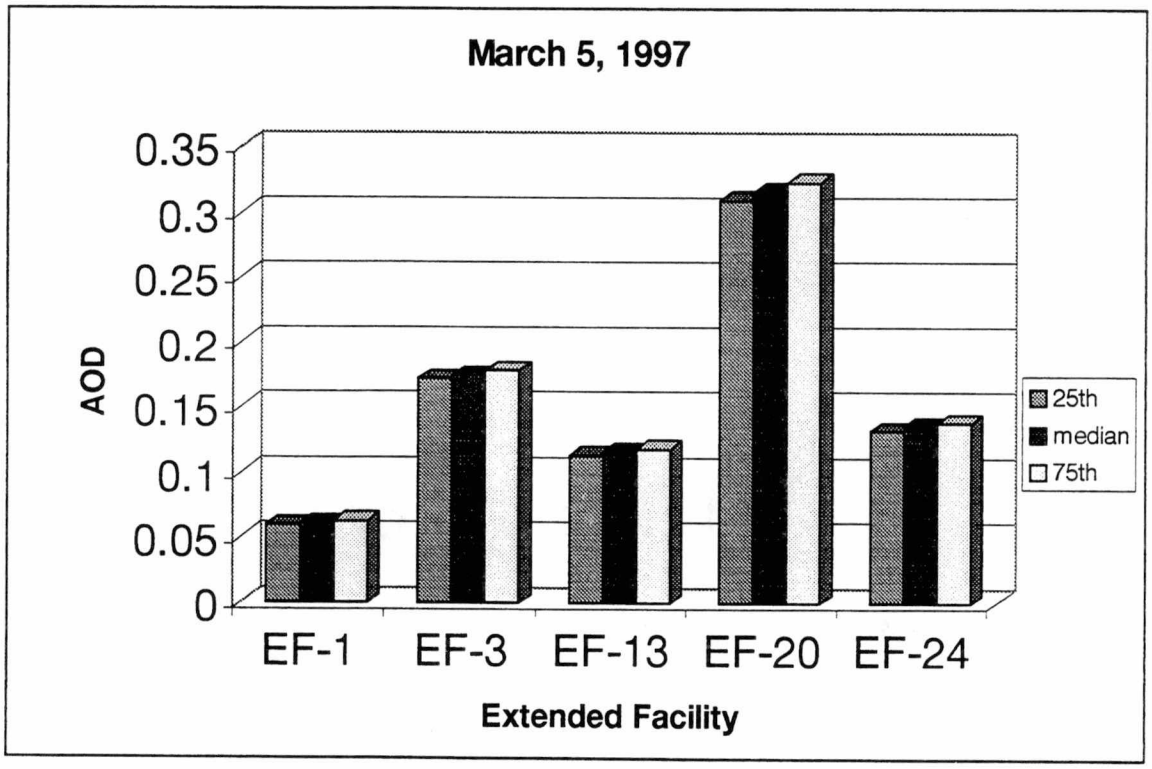

Figure 25. IQR of AOD for Morning of March 5, 1997 at all Facilities

The pair-wise Pearson correlation coefficients were calculated in an effort to quantify spatial similarities/differences. The Pearson coefficients found in Table 3, ranged from 0.49 (EF-1 vs. EF-3) to 0.96 (EF-20 vs. EF-24). The correlation coefficients indicated that EF-1 was not highly correlated with the other four facilities. EF-1 was located at the northwest corner of the CART site (Figure 1).

To verify that EF-1 was not correlated with the other facilities a varimax-rotated Principal Components Analysis (PCA) was performed. The eigenvalues after a varimax rotation in Table 4 indicated that the first two factors were significant and that they explained 90.5% of the AOD variation within the CART site. The next largest eigenfactor explained only an additional 6.5% of the total variance. The factor loadings in Table 5 demonstrated that the first factor described the variation at EF-3, 13, 20 and 24.

Thus, the patterns of variability at these four facilities were similar. This suggests that the aerosols described by Factor 1 originated from a single source area, likely a long distance

Table 3. Pair-wise Pearson coefficients for all AOD

	EF-1	**EF-3**	**EF-13**	**EF-20**	**EF-24**
EF-1	1.0				
EF-3	0.49	1.0			
EF-13	0.71	0.88	1.0		
EF-20	0.67	0.93	0.92	1.0	
EF-24	0.67	0.90	0.95	0.96	1.0

Table 4. PCA Eigenvalues for all AOD.

NUMBER	EIGENVALUE	INDIVIDUAL PERCENT	CUMULATIVE PERCENT
1	**3.03**	60.61	60.61
2	**1.49**	29.88	90.49
3	0.33	6.53	97.02
4	0.10	2.00	99.02
5	0.05	0.98	100.00

away from the CART site. In contrast, Factor 2 described 95% of the variation at facility EF-1. The second factor showed that the EF-1 variations were unique, which implies that the origin of the aerosols measured were different from those of the other facilities. Both the Pearson correlation coefficients and PCA confirm that the variations at EF-1 were dis-similar to the other facilities at the CART site.

The spatial variability of AOD at 4 of the 5 facilities was similar, however when the morning and afternoon AOD values are separated some interesting variations were observed. The Pearson correlation coefficients for just the morning or afternoon in Table 6 indicated that there were some differences in the variations in the morning and afternoon.

Table 5. PCA Factor Loadings for all AOD

FACILITY	FACTOR 1	FACTOR 2
EF-1	-0.29	**-0.95**
EF-3	**-0.97**	-0.21
EF-13	**-0.75**	-0.44
EF-20	**-0.87**	-0.42
EF-24	**-0.82**	-0.39

Table 6. Pearson Correlation Coefficients: Morning and Afternoon

MORNING					
	EF-1	**EF-3**	**EF-13**	**EF-20**	**EF-24**
EF-1	1.0				
EF-3	0.54	1.0			
EF-13	0.81	0.88	1.0		
EF-20	0.78	0.91	0.93	1.0	
EF-24	0.82	0.89	0.97	0.97	1.0
AFTERNOON					
	EF-1	**EF-3**	**EF-13**	**EF-20**	**EF-24**
EF-1	1.0				
EF-3	0.15	1.0			
EF-13	0.44	0.27	1.0		
EF-20	0.58	0.24	0.69	1.0	
EF-24	0.03	0.14	0.48	0.61	1.0

The same PCA analysis was performed separately on the morning and afternoon data sets. The morning PCA showed that there was two significant eigenvalues and they describe 95% of the variation in the morning AOD. The morning factor loadings in Table 8 indicated that the first factor described the variations at EF-3, 13, 20 and 24 similar to the previous PCA of the AOD values for the entire day.

Table 7. PCA Eigenvalues for Morning AOD.

NUMBER	EIGENVALUE	INDIVIDUAL PERCENT	CUMULATIVE PERCENT
1	**2.81**	56.28	56.28
2	**1.95**	39.02	95.30
3	0.15	3.01	98.32
4	0.05	1.00	99.32
5	0.03	0.68	100.00

Table 8. PCA Factor Loadings for Morning AOD

FACILITY	FACTOR 1	FACTOR 2
EF-1	-0.31	**-0.95**
EF-3	**-0.97**	-0.24
EF-13	**-0.74**	-0.58
EF-20	**-0.81**	-0.56
EF-24	**-0.76**	-0.59

The factor loadings in the morning are very similar to those of the combined morning and afternoon AOD values previously shown in Table 5. Factor 2 only describes the variation of AOD at EF-1. The pattern of AOD variation at the other four facilities was again similar.

The afternoon varimax-rotated PCA showed some surprising results. The afternoon eigenvalues are shown in Table 9. In using the criteria that an eigenvalue less than one is insignificant there appeared to be four significant factors, however the percent variation for each factor showed that the fifth factor was significant. Therefore, five factors for the afternoon AOD values were significant. Analysis of the afternoon factor loadings in Table 10 indicated that each factor describes the variations at only one facility. This

Table 9. PCA Eigenvalues for Afternoon AOD.

NUMBER	EIGENVALUE	INDIVIDUAL PERCENT	CUMULATIVE PERCENT
1	1.15	22.94	22.94
2	1.13	22.63	45.57
3	1.02	20.32	65.89
4	1.05	20.92	86.81
5	0.66	13.19	100.00

Table 10. PCA Factor Loadings for Afternoon AOD.

FACILITY	FACTOR 1	FACTOR 2	FACTOR 3	FACTOR 4	FACTOR 5
EF-1	0.03	**-0.96**	0.07	0.20	0.19
EF-3	-0.05	-0.06	**0.99**	0.11	0.06
EF-13	-0.25	-0.23	0.13	**0.91**	0.21
EF-20	-0.41	-0.39	0.11	0.36	**0.73**
EF-24	**-0.95**	-0.03	0.06	0.22	0.20

demonstrated that the pattern of variation in the afternoon AOD across the CART site was not consistent from facility to facility. Each facility varied independently of all other facilities. These afternoon variations were likely due to variations in local sources of aerosols produced by activities such as farming.

5. CONCLUSIONS AND RECOMMENDATIONS

Characterization of the AOD reported here provides clear evidence that spatial and temporal variation across the spatial extent of the ARM SGP CART site. The monthly median AOD showed a clear seasonal pattern at all five facilities, with minimum values in the winter and maximums in the summer. The morning mean and median AOD values were 8 to 57% higher than the afternoon mean and median AOD. Correlation coefficients and the varamax-rotated PCA suggested that the morning AOD vary consistently across the site with the exception of EF-1. The PCA also indicated the afternoon AOD variations were unique at each facility studied. Finally, the magnitude of AOD variation was different across the facilities.

In short, the magnitude of the spatial and temporal variation were substantial within the site. This variability may have significant impacts on regional and local radiative transfer and GCM predictions. This sub-GCM grid variation cannot be ignored if the model is to be used to accurately predict future climate change. Improved parameterization is needed to incorporate aerosol processes into the next generation GCMs.

REFERENCES

REFERENCES

1. 40CFR50
2. Smaglik, P. *Scientist* 1998. *12-1* 1
3. Stokes, G.M.; Schwartz, S.E. *Bulletin of the Amer. Met. Soc.* 1994. *75(7).* 1201-1221.
4. *Atmospheric Aerosols*, Twomey, S., Elsevier Scientific Publishing: Amsterdam, 1977.
5. Halthore, R.N.; Schwartz, S.E.; Michalsky, J.J.; Anderson, G.P.; Farrare, R.A.; Holben, B.N.; Ten Brink, H.M. *J. of Geophys. Res.* 1997. *102-D25.* 29,991-30,002
6. Penner, J.E.; Charlson, R.J.; Hales, J.M.; Laulainen, N.S.; Leifer, R.; Novakov, T.; Ogren, J.; Radke, L.F.; Schwartz, S.E.; Travis, L. *Bulletin of the Amer. Met. Soc.* 1994. *75(3).* 375-400
7. Internet Web Page Uniform Resource Locator (URL) - http://www.archive.arm.gov/
8. Cheng, M.D.; Nash, T.M. Kopetz, E.S. *J. Aerosol Sci.*, in review.
9. Cheng, M.D., Hubbs, C.; McCord, R. *EOS /American Geophys. Union.* 1996. 493
10. Harrison, L.; Michalsky, J.; Berndt, *J. Appl. Optics.* 1994, *33-22*, 5118-5125
11. *Atmospheric Radiative Transfer*, Lenoble, J., A. DEEPAK Publishing: New York, NY, 1993.
12. Kasten, F. *Arch. Meterol. Geophys. Bioklimatol.* 1965. *B 14.* 206-223
13. *Aerosol Technology*, Hinds, W. C., John Wiley & Sons, Inc., New York, NY, 1982.
14. *Robust Regression and Outlier Detection*, Rousseeuw, P.J.; Leroy, A.M., John Wiley & Sons: NewYork, 1987.
15. Harrison, L.C.; Michalsky, J.J. *Appl. Optics.* 1994, *33-22* 5126-5132
16. Teillet, P.M. *Appl. Optics.* 1990, *29-13*, 1897-1900

17. Hansen, J.E.; Travis, L.D. *Space Sci. Rev.* 1974, *16*, 527

18. Internet Web Page URL - http://www.arm.gov/docs/instruments/static/smos.html

19. Internet Web Page URL - http://www.cmdl.noaa.gov/dobson

20. Internet Web Page URL - http://jwocky.gscf.nasa.gov/dobson.html/

21. Michalsky, J.J.; Liljegren, J.C.; Harrison, L.C. *J. of Geophys. Res.* 1995, *100-D12*, 25,995-26,003

22. Shettle, E.P.; Anderson, S. *Proceedings of the 17th Annual Review Conference on Atmospheric Transmission Models*, June 1994, 335-345

23. Michalsky, J.J., State University of New York, Albany , personal communication, 1998

24. Smirnov, A.; O'Neill, N.T.; Royer, A.; Tarussov, A. *J. of Geophys. Res.* 1996, *101-D14* 19,299-19,318

25. Devara, P.C.S.; Pandithurai, G.; Rja, R.E.; Sharma, S. *J. Aerosol Sci.* 1996, *27-4*, 621-632

26. Michalsky, J.J.; Schlemmer, J.A.; Larson, L.C.; Harrison, L.C.; Berkheiser, W.E.; Laulainen, N.S. *Proceedings of the Air and Waste Management Association Visual Air Quality and Atmospheric Radiation Conference*, 1994.

APPENDIX

APPENDIX

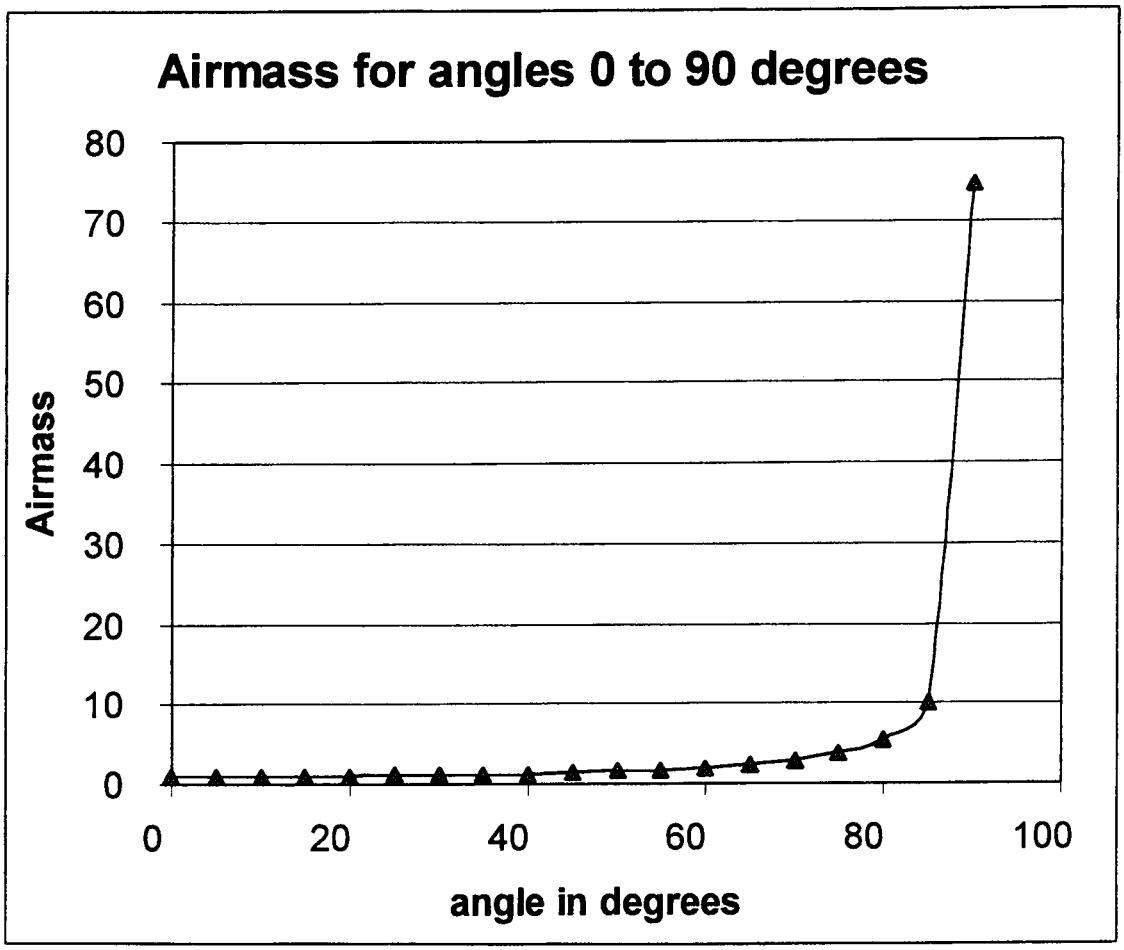

Figure A1. Airmass for Angles 0° to 90°.

VITA

Terra Nash was born June 6, 1973 in Idaho Falls, ID and grew up in nearby Blackfoot, ID. She graduated form Blackfoot High School in May of 1991. That fall she began attending Utah State University in Logan, UT. In June 1996 Terra received a BS in Environmental Engineering from USU. She began her masters work at the University of Tennessee in January 1997. In May of that year, she began a research internship at Oak Ridge National Laboratory. Terra received her Environmental Engineering MS degree in December of 1998.